Lymphocyte genes and an enhancer sequestered at the nuclear periphery undergo constrained release and associate upon T-cell activation

Michael I. Robson, Jose I. de las Heras, Alastair R. W. Kerr and Eric C. Schirmer

The Wellcome Trust Centre for Cell Biology and Institute of Cell Biology, University of Edinburgh, Edinburgh EH9 3BF, UK

Correspondence to:

Eric Schirmer

Wellcome Trust Centre for Cell Biology

University of Edinburgh, Kings Buildings

Swann 5.22, Max Born Crescent

Edinburgh EH9 3BF, UK

Tel:+44(0)1316507075

Fax:+44(0)1316507360

e.schirmer@ed.ac.uk

Abstract

The 3D organization of the genome changes concomitantly with expression changes during hematopoeisis and immune activation. However, studies of this phenomenon have focused either on topologically associated domains (TADs) or on lamina-associated domains (LADs) with few studies investigating how TADs and LADs affect one another. To address this we employed a Jurkat T-cell activation system. Lamin B1-DamID was first performed on the resting and activated cells to globally identify all genes moving between the nuclear periphery and the nuclear interior. This identified changes in gene positioning in both directions, though genes being released from the periphery significantly dominated. To assess whether these changes at the nuclear periphery influence wider genome organization, the genes changing in our DamID datasets were contrasted with topologically associated domains (TADs) identified with high resolution in the GM12878 lymphoblastoid cell line. We selected genes that occurred in both LADs and TADs that were released from the periphery during lymphocyte activation. These were tested by fluorescence in situ hybridization finding that the whole TAD moves when an overlapping LAD changes during Jurkat activation and also that higher order TAD compartment interactions are altered. In particular, release of an enhancer from the periphery in the activated cells enabled its association into a higher order TAD-TAD compartment structure. Thus, while TADs are the fundamental unit of genome organization, altered lamina associations clearly influence inter-TAD gene-enhancer interactions as an important additional mode of gene regulation during T-cell activation.

Introduction

The genome is non-randomly organized within the three-dimensional space of the interphase nucleus. At one level, regulatory elements influence the activity of target genes many hundreds of Kb to many Mb distal by moving into close proximity through looping in three-dimensional space (Arner et al., 2015; Sanyal et al., 2012; Schoenfelder et al., 2015; Shen et al., 2012). Chromosomes are also organized along their length into discrete large genomic regions termed topologically associated domains (TADs) that display more frequent interactions within the domain than with the rest of the genome (Dixon et al., 2012; Hou et al., 2012; Nora et al., 2012; Sexton et al., 2012). In general, the topological constraints imposed by TADs limit the propensity of looping interactions to *cis*-regulatory element:gene pairings present within the same domain (Hnisz et al., 2016). However, a higher level of TAD organization also occurs in which multiple TADs that are many Mb distal or on different chromosomes can also be adjacent in the higher order folding of the genome (Rao et al., 2014). Indeed, although less frequent than intra-TAD interactions, a number of inter-chromosomal and inter-TAD interactions are consistently observed with chromosome conformation capture (Hi-C) approaches. Similarly, inter-chromosomal loci interactions have been observed by FISH involving genes that are co-regulated during differentiation (Neems et al., 2016; Schoenfelder et al., 2010). However, how inter-TAD interactions are controlled during differentiation or other cellular transitions is largely unexplored.

A completely different level of radial genome organization occurs with respect to the nuclear periphery. A polymer of nuclear lamins lines the inner surface of the nuclear membrane and so-called lamina-associated domains (LADs) define genome regions at the nuclear periphery (Vogel et al., 2007). However, lamins are not required for tethering genome regions to the periphery (Amendola and van Steensel, 2015). The nuclear periphery is a generally repressive environment with genes in LADs tending to overlap with late-replicating DNA lacking active histone marks and containing many silencing marks (Pickersgill et al., 2006; Pindyurin et al., 2007). Many LADs are constitutive, occurring in all

cells investigated thus far, but as more cell types are investigated the subset of facultative LADs that change in their peripheral associations either during the cell cycle or between cell types is constantly increasing (Kind et al., 2013; Kind and van Steensel, 2014; Meuleman et al., 2013; Peric-Hupkes et al., 2010; Robson et al., 2016). The importance of facultative LADs is underscored by the fact that knockdown of nuclear membrane proteins involved in the peripheral tethering of some facultative LADs has profound negative consequences for tissue differentiation (Robson et al., 2016). Tellingly, these facultative LADs often contained genes requiring fine-tuned regulation in differentiation and genomic regions both moving to and from the periphery during differentiation (Peric-Hupkes et al., 2010; Robson et al., 2016).

Few studies have investigated the relationship between these two types of genome organization, but there are many important questions that come to mind. Does a TAD as a functional unit move between the periphery and interior and thus perhaps encompass or be contained within a facultative LAD? Can a new LAD that forms during differentiation break up a TAD or long-range inter-TAD interaction by sequestering a gene or enhancer at the periphery or vice-versa?

The movement of genes in facultative LADs between the nuclear periphery and the nuclear interior tends to be associated with their repression or activation respectively. In neurogenesis and myogenesis 5-15% of genes move from the nuclear periphery to the interior while another 5-10% move from the interior to the periphery (Peric-Hupkes et al., 2010; Robson et al., 2016). Genes moving to the periphery in myogenesis tended to be needed at early stages in myogenesis and inhibitory at later stages, thus requiring more fine-tuned regulation (Robson et al., 2016). Moreover, several of the genes under this type of regulation are normally re-activated in muscle repair after injury. Similarly in lymphocyte differentiation several gene-positioning changes have been observed such as release of the *IgH* locus from the periphery upon induction of *V-D-J* recombination (Kosak et al., 2002) and

movement of the *c-maf* locus to the periphery with its repression (Hewitt et al., 2004), though a global profiling of changes during lymphocyte differentiation has not been reported.

Lymphocyte activation in contrast to differentiation is a much more rapid and dynamic process associated with massive genome restructuring (Drings and Sonnemann, 1974). Compacted chromatin in the resting stage dissipates in the activated state concomitant with large-scale gene activation (Pompidou et al., 1984). This raised the question of whether the massive gene activation and chromatin decondensation in lymphocyte activation is uni-directional or whether there is an exchange of genes tethered at the nuclear envelope as in differentiation. We anticipated that some level of regulation occurs from nuclear membrane proteins because changes in the protein composition of the nuclear membrane were observed during lymphocyte activation (Korfali et al., 2010). Furthermore the strong activation of genes during lymphocyte activation suggested the hypothesis that the nuclear envelope could help maintain the resting state not only by peripheral gene positioning, but also by sequestering enhancers to keep them away from target genes.

To address these questions we first used lamin B1-DamID to globally identify changes in genome contacts with the nuclear periphery in resting and activated Jurkat T-cells, finding that indeed there is an exchange of genome contacts as opposed to a whole-scale release from the periphery. Moreover, many of the genes under this control by the nuclear envelope are important genes for immune responses. Comparison of the DamID data with Hi-C datasets from the GM12878 lymphoblastoid cell line revealed that lamin B1 peripheral contacts are under represented in the Hi-C data. However, where the same genome regions were represented in both datasets the boundaries of TADs and LADs were comparable. Most importantly, changes in LADs influenced the higher order organization of TADs: when TADs corresponded to LADs at the periphery they were maintained physically separate while after LAD dissociation and release from the periphery these TADs co-assembled into a higher order compartment. Interestingly, an enhancer in a LAD at the periphery in resting Jurkat cells was released from the periphery upon lymphocyte activation

and then was able to associate with immune activation genes that had been kept apart when also at the periphery in the resting lymphocytes. Thus changes in LADs can influence the internal association between TADs in an important contribution to immune gene activation.

Results

Mapping Gene Expression and Repositioning Changes during T-cell Activation

The extensive electron dense peripheral heterochromatin found in resting T-cells dissipates during activation concomitantly with the induction of immunogenic genes (Hirschhorn et al., 1971; Manteifel et al., 1992; Pompidou et al., 1984; Rawlings et al., 2011). We predicted that the dissipation of peripheral heterochromatin would specifically correlate with a release of T-cell activation-associated genes from the periphery. Accordingly, we investigated coordinated gene expression and genome organization changes during T-cell activation using microarrays and DamID (Fig. 1). Jurkat cells were incubated with Raji B-cells that had been pre-conjugated with staphylococcal enterotoxin E (SEE) resulting in the formation of antigen-independent immunological synapses as has been reported previously (Fig. 1A) (Gonzalez-Granado et al., 2014). This yielded robust activation of over 95% of Jurkat cells as assessed by CD69/CMAC fluorescence activated cell sorting (FACS) (Fig. 1B). To determine gene expression changes associated with activation, RNA was extracted at 0, 8, 24 and 48 h post-SEE stimulation and analyzed on Illumina bead microarrays. Upon activation, 1,112 genes were upregulated at least 1.4-fold and these were significantly enriched in GO-terms positively supporting T-cell activation and early effector function (Figure 1C, S1). Similarly, 1,016 genes were repressed at least 1.4-fold and these were significantly enriched in GO-terms inhibiting mitosis and cell division, presumably in order to permit accelerated proliferation of activated cells. Thus, both FACS and GO-term analysis confirmed efficient Jurkat T-cell activation.

The same cell populations were subjected to lamin B1-DamID to map global changes in associations between genomic loci and the nuclear periphery in resting and activated Jurkat cells (Fig. 1D, E). Bacterial Dam methylase fused to lamin B1 was delivered to cells by lentiviral transduction where it could provide its unique methylation to DNA proximal to the lamin polymer that underlies the inner nuclear membrane (Vogel et al., 2007). The methylated DNA was then isolated and identified by next generation sequencing. To control for local variation in chromatin accessibility, soluble Dam methylase was expressed in parallel experiments. As time course experiments reveal no DamID signal until roughly 48 h after lentiviral transduction, Jurkat cells were transduced with DamID constructs 24 h before antigen presentation so that the measured changes reflect the genome organization between 24 and 48 h into Jurkat activation (Fig. 1A).

Log2(Lamin B1 Dam/soluble Dam) ratios were generated and used to identify lamina associated domains (LADs) in resting and activated Jurkat T-cells based on a circular binary segmentation algorithm with slight modifications from that previously described ((Harr et al., 2015); see materials and methods). Interestingly the magnitude of changes were similar between this rapid activation system and previous DamID studies of differentiation investigating neurogenesis and myogenesis (Peric-Hupkes et al., 2010; Robson et al., 2016) with the majority of LADs maintained between resting and activated cells. 94% of the LAD coverage was shared between resting and activated cells with the remaining 6% roughly equally distributed between lost and newly formed LADs (Fig. 2A). Moreover, the 16.2% of genes found within LADs were less transcriptionally active than the 83.8% of genes found in non-LADs (Fig. 2B), in line with other studies representing the periphery as a repressive environment (Pickersgill et al., 2006; Pindyurin et al., 2007).

The Jurkat Genome Is Pre-configured for T-Cell Activation

Interestingly, the types of genes found in LADs in the resting state correlated with certain categories of lymphocyte genes based on their transcriptional behaviour (Best et al., 2013). In this study an extensive time course of mouse $CD8^+$ T-cell gene expression changes in response to antigen stimulation revealed 10 categories of genes with distinct transcriptional behaviors. Gene classes involved in early stages of activation such as cell cycle progression and early/short term effector function were significantly depleted from LADs relative to the whole genome and displayed increased gene expression (Fig. 1C). In contrast, classes not needed until later in T-cell responses such as those associated with naive, late effector and memory T-cell function were found in LADs as frequently as the whole genome and were mostly transcriptionally repressed (Fig. 1C). This both validates our data in its correspondence with previous studies of T-cell activation and demonstrates the biological significance of gene regulation from the nuclear lamina.

Considering all genes from our Jurkat activation microarray data, only 4-5% of induced and repressed genes were observed in LADs in resting cells (Fig. 2D). Paralleling this depleted association with the periphery, both induced and repressed genes also possessed significantly high basal levels of expression in resting Jurkat T-cells (Fig. 2E). Hence, the resting T-cell genome appears to be in a more preconfigured state with genes that are immediately induced or repressed being positioned away from the nuclear periphery with a higher level of basal expression than the remaining genome.

T-cell critical genes are released from the periphery and induced during T-cell activation

To further investigate this 4-5% of induced or repressed genes starting in LADs at the periphery in resting cells, we re-evaluated the DamID data for specific gene repositioning. However, a binary LAD or non-LAD definition often fails to identify such positioning changes

(Peric-Hupkes et al., 2010; Robson et al., 2016). Such changes are reflected instead by an increased or decreased signal intensity from the log2(Lamin B1/Dam) ratio (Kind et al., 2015; Peric-Hupkes et al., 2010; Robson et al., 2016). Hence, we applied an established statistical method (Robson et al., 2016) to identify regions that exhibit significant changes in peripheral association in resting and activated Jurkat T-cells. Whereas ~40% of the genome could be found in LADs in both resting and activated Jurkat T-cells, only ~2-4% of the genome was found in regions changing significantly in the log2(Lamin B1/Dam) signal intensity (Fig. 3A). A tendency to increase association with the periphery in activated cells versus resting cells (denoted 'IP') was observed for 2.1% of the genome in 1,070 regions with a median size of 52 Kb containing 157 genes. The opposite tendency (decreasing association from the periphery; 'PI') was observed for 3.5% of the genome in 2,969 regions with a median size of 47 Kb, covering containing 799 genes (Fig. 3A). An example of the intensity shift for genes in PI regions is shown in Figure 3B. Hence, paralleling the dissipation of peripheral heterochromatin, more of the genome displays decreased association with the periphery than increased association during T-cell activation.

Of the 4-5% of genes found in LADs in resting Jurkat cells that became induced during activation, ~48% displayed reduced peripheral association during T-cell activation compared with 23% for the whole genome (Fig. 3C). This is consistent with the periphery functioning as a repressive environment. In the opposite direction, of genes found in LADs in resting Jurkat cells that became repressed during activation, 12% displayed increased peripheral association compared with 4% for the whole genome (Fig. 3C). Nonetheless, while associated with transcriptional repression, the majority genes moving to or from the nuclear periphery displayed no change in expression (Fig. S2A). Interestingly, while the trend was the same in a recent study on myogenesis, the extent to which repositioning was associated with altered gene expression was much less than here for lymphocyte activation (Fig. S2A).

The genes undergoing repositioning tended to be important for T-cell regulation. To confirm their decreased peripheral association inferred from DamID six such genes were selected for direct testing by fluorescence *in situ* hybridization (FISH). These were the guanylate binding protein (GBP) gene cluster, Cbl proto-oncogene B (*CBLB*), CD200 molecule (*CD200*), B and T lymphocyte associated (*BTLA*), interleukin 2 (*IL2)* (Fig. 3D) and the vascular cell adhesion molecule 1 (*VCAM1*) (Fig. S2B). FISH was performed in resting and activated Jurkat T-cells together with lamin B2 staining to identify the edge of the nucleus. The absolute distance between the peak fluorescence intensity of lamin B2 and the gene was measured in the mid-plane from deconvolved wide-field images and plotted as a cumulative frequency plot. In such plots increasing distances from the lamina are viewed as a shift to the right. The use of absolute distances did not skew results based on altered nuclear size because no significant nuclear volume changes were observed between the resting and activated Jurkat T-cells (data not shown). The directly measured gene positions for the GBP cluster, *CBLB*, *CD200* and *BTLA* all matched the peripheral positioning predicted by the DamID in resting cells and were released during activation (Fig. 3E,F). In all cases the differences were highly statistically significant by Kolmogorov-Smirnov test. We selected the *VCAM1* gene because, unlike the others, it is encompassed within a PI region while the LAD it is contained within also has additional PI and IP regions. Interestingly, with these conflicting parameters *VCAM1* did not reposition (Fig. S2B) and thus serves as a control showing that not all genes reposition away from the periphery during activation. The *IL2* gene was tested because, although failing to pass the statistical threshold for a PI region, the LAD boundaries diminish. The *IL2* position also changed, suggesting that the threshold set for the IP/PI selection is sufficient to trust all positive selected repositioning events but misses some differences close to the signal to noise ratio. An internally positioned gene induced during T-cell activation, the IL2 receptor subunit alpha (*IL2RA/CD25)*, was used as an additional control that specific locus-peripheral interactions and not larger-global interactions were being measured and accordingly no significant repositioning with respect to the periphery was observed (Fig. S2C).

The measurement of absolute distances allowed several interesting comparisons in these data. For example, the GBP cluster that has large adjacent non-LADs compared with the other genes sampled was able to reach a greater distance away from the nuclear periphery (up to 0.89 μm) than the other genes tested (up to 0.6 μm) that are flanked by more proximal LADs maintained through T-cell activation (Fig. 3F). Secondly, the final distance away from the periphery adopted by the GBP cluster upon activation is very similar to the activated distance from the periphery (0.85 μm) of *IL2RA/CD25* that displays no lamina association by DamID ($p = 0.727$, KS test). Thus, the distance from the periphery adopted by a gene in both resting cells and following activation-induced repositioning is dependant upon the surrounding genomic environment.

Topologically Associated Domains form the unit of gene repositioning

Many recent studies have revealed that the internal nuclear organization is as functionally important as peripheral organization. Thus, we were interested in determining the relationship between regions moving away from the periphery and TADs. The relationship between LADs and TADs is unclear with several studies reporting significant but only partial overlap between TAD and LAD boundaries (Dixon et al., 2012; Fraser et al., 2015; Kind et al., 2015). However, the degree to which regions with altered peripheral localization are delimited to single TADs or span multiple TADs has yet to be tested.

To investigate this we contrasted the DamID maps of resting and activated Jurkat T-cells to the published GM12878 lymphoblastoid cell line Hi-C contact map (Rao et al., 2014). The 950 bp resolution of the GM12878 Hi-C map is the highest yet achieved, thus permitting detailed domain delineation. This is also enabled by use of a different methodology (Contact Domains) from the commonly used directionality index to define TAD domains. Global analysis of TAD and LAD distributions between the GM12878 Hi-C map and our DamID dataset for resting and activated Jurkat T-cells revealed that LADs are frequently contained

in their entirety within TADs. This was the case for both resting and activated LADs (Fig. S3). To test this possibility 500 LADs were randomly selected and tested for their complete envelopment within TADs. As a control this was contrasted to an identically treated randomly shuffled genome control. The LAD and control shuffled selections of 500 regions per iteration were repeated over 1,000 iterations and the frequencies of LAD envelopment within TADs plotted (Fig. S3). Both resting and activated LADs occurred in TADs more frequently than for the shuffled genome iterations and little or no difference was observed between the resting and activated LADs. We postulate that this observed increase in the expected frequencies of LADs found completely within TADs indicates that when a TAD contains a region of altered peripheral association the TAD repositions as a unit.

First, to test that TAD structure is similar in GM12878 cells and Jurkat T-cells, we chose 5 fosmid probes that were each 174 Kb distance from each other in series over the *VCAM1* locus. The first was in a neighboring TAD upstream of *VCAM1*, the second just within the *VCAM1* TAD boundary, the third directly in the TAD center, the fourth just within the TAD boundary downstream of *VCAM1*, and the fifth downstream in a neighboring TAD (Fig. 4A). The percentage of significant probe co-localization for different probe pairs was determined from max projection deconvolved images taken by widefield fluorescence microscopy. Supporting the similarity between the TAD structure in GM12878 cells and Jurkat T-cells, the probe set contained within the same TAD exhibited higher significant co-localization than the probe sets between adjacent TADs (Fig. 4B).

To test whether a TAD is the unit of repositioning or if its structure changes during lymphocyte activation-induced gene repositioning, FISH was performed on resting and activated T-cells using a similarly generated set of 5 FISH probes (except 149 Kb distant from one another) covering the GBP gene cluster (Fig. 4C). Again, higher significant co-localization was observed for within the TAD than between adjacent TADs and this organization was maintained between both the resting and the activated state (Fig. 4D).

Hence, at least in this instance, the unit of repositioning is the TAD and it remains unaltered following repositioning.

Release of a T-cell activation specific enhancer from the nuclear periphery enables its association with target genes in the interior

Several of the genes we tested to confirm release from the periphery concomitant with their induction during Jurkat T-cell activation (*CBLB*, *BTLA* and *CD200*; Fig. 3) were within a 20 Mb region along chromosome 3. The Hi-C map from the GM12878 cells indicated that these loci, though many Mb apart, display higher-order inter-TAD interactions (Fig. 5A). Compellingly, an extensive long-range contact was observed between these released genes and another 66 Kb region displaying a similarly decreased peripheral association during T-cell activation. This region contained no obvious genes but displayed characteristics of an enhancer induced during T-cell activation: in particular the released region displayed significantly elevated levels of H3K4me1 and H3K27ac in published ChIP-seq from GM12878 cells (Fig. 5B) (Consortium, 2012). Moreover, published ChIP-seq data from the Reference Epigenome Mapping consortium from resting and Phorbol 12-myristate 13-acetate (PMA)-stimulated human $CD4^+$ T-cells revealed H3K27ac levels drastically increase at this region following T-cell activation (Bernstein et al., 2010), suggesting the putative enhancer becomes specifically activated in T-cells concomitantly with its release from the periphery. Finally, supportive of the 66 kbp released region containing an enhancer, a recent study mapping enhancers using H3K27ac identified this region as a cluster of enhancers, sometimes referred to as a super-enhancer, specifically active in activated T-cells (Hnisz et al., 2013).

While TAD boundaries frequently isolate enhancers with their target genes, inter-TAD enhancer-gene interactions have also been observed (Andrey et al., 2013; Plank and Dean, 2014). Therefore, we hypothesized that the occurrence of this enhancer in a distinct upstream TAD at the periphery served to prevent its premature association with the target

genes until released from the periphery during T-cell activation. We predicted that the physical distance between the enhancer and its presumptive Mb-distal target genes would be reduced as they begin interacting during T-cell activation. We first confirmed that the enhancer was released from the periphery during T-cell activation, finding it was (Fig. 5C). At the same time we also tested the positioning of the *NFKBIZ* locus, which was induced during T-cell activation, similarly displayed long-range Hi-C interactions with the enhancer and was proximal to but not immediately overlapping with a PI region. Though only immediately proximal to a LAD, this locus was close to the periphery in resting cells and became more internal during activation, indicating again that genomic context is important to consider in addition to lamina-association as determined by DamID (Fig. 5C).

To test for altered enhancer-gene interactions, FISH was performed on combinations of the enhancer probe with the individual gene probes (*NFKBIZ*, *CBLB*, *CD200*, and *BTLA*) in both resting and activated cells. For all combinations the distance, as measured by max-projection in 3D, was reduced upon activation (Fig. 5D). By contrast, the similarly spaced GBP cluster and *VCAM1* locus (11 Mb apart), which display no clear Hi-C interactions, exhibited no significant change in 3D spatial distance upon activation (Fig. S4). Likewise, the *IL2* and *IL2RA/CD25* loci that are located on separate chromosomes and are therefore much further apart in three-dimensional space did not exhibit any significant change in the distance between them.

A majority of peripherally sequestered enhancers are released from the periphery concomitantly with induction of T-cell activation

To gauge the pervasiveness of this mode of regulation of enhancer activity from the nuclear periphery, a list of enhancer clusters/super-enhancers functioning during T-cell activation were extracted from a previous study (Hnisz et al., 2013) and compared to the DamID data for Jurkat activation. Of the nearly 1,000 super-enhancers, 354 were active in both states,

107 were active only in resting T-cells, and 513 were induced only in activated T-cells (Fig. 6A). Of those induced during T-cell activation, only 32 occurred in LADs in the resting Jurkat T-cells. However, over half of these were released from the periphery in the activated Jurkat T-cells (Fig. 6B). Hence, similar to genes, peripherally positioned enhancers are released concomitantly with their activation and acquisition of H3K27ac during T-cell activation.

Discussion

Peripheral constraints restrict mobility in resting T-cells, but enhance interactions upon activation

TADs generally contain both the enhancer and its target genes and so isolate them to prevent the enhancer from acting on inappropriate targets (Hnisz et al., 2016; Lupianez et al., 2015). We now show here a new mode of regulation wherein lamina association isolates and sequesters the enhancer away from target genes in multiple TADs. Upon lymphocyte activation these TADs are released from the periphery; however, adjacent constitutive LAD regions between the released TADs are maintained at the periphery. This limits the distance from the periphery in a way that increases the probability of enhancer-gene interactions: two chromatin regions looping out from the nuclear envelope of similar distance and tethered close to one another would be much more likely to interact than one loop of 5 Mb and another of 30 Mb. Indeed, the *CBLB* locus, the *CD200* locus and the enhancer were all in regions of roughly 4 Mb containing small weaker LADs that were separated by very strong long unbroken LADs.

Once released these TADs remained relatively close to the periphery, never moving further than ~0.6 μm (Fig. 3). This is an important consideration because modelling studies indicate that it is unlikely for TADs to find each other in a single cell cycle by diffusion alone if they are 10 Mb apart (Dekker and Mirny, 2016). This modelling predicted that ~0.5-0.8 μm space could be sampled by a locus in 1 h, well within the rapid response timeframe for

lymphocyte activation and the distance we observed between the enhancer and target gene following their constrained release from the periphery (0.4-0.59 μm; Fig.5). Thus, at one level the constraints on movement after release from the periphery place enhancer and target genes in proximity to increase the probability of assembly into a higher order chromosome compartment while at the same time restricting them away from other inappropriate targets.

At a second level, in resting cells the TADs at the periphery are limited in mobility and maintained apart. Indeed, while dynamic exchange of LADs has been reported (Kind et al., 2013), chromatin at the nuclear envelope remains far less dynamic than that in the nuclear interior (Chubb et al., 2002; Strickfaden et al., 2010). Hence, the peripheral association of enhancer and target gene TADs limits their sampling of 3D space and forming function interactions. By being restricted to a 2-dimensional surface the enhancer and target gene TADs have a limited ability to topologically associate thereby forming a linear array of TADs at the nuclear lamina. This is consistent at least for the example of the enhancer-gene interactions shown here in that the distance measured from the enhancer to the 4 Mb distal *NFKBIZ* locus was 0.54 μm in the resting cells while the 8 Mb distal *CBLB* locus was 0.86 μm, as would be expected from a linear association. Once released, however, the DNA regions in between could loop out so that the TADs could assume a topological organization to directly interact at an internal interface. By keeping them close but apart at the periphery they should be sufficiently constrained to make it easier to find each other for self-assembly upon release and allow rapid activation.

Genes subject to spatial regulation are critical for T-cell activation

In an earlier study of myogenesis the genes specifically regulated from the nuclear envelope were often required in the initial stages of differentiation, but needed to be tightly shut off later because they were inhibitory at later stages (Robson et al., 2016). Similarly, here the

genes subject to spatial regulation (Figures 3 and 5) were important for T-cell function, but the first responder genes that initiate activation were strongly absent from LADs (Fig. 2). Several of the spatially regulated genes associated with this enhancer function in modulating the activation response. For example, *NFKBIZ* encodes an inhibitor of the transcription factor NFkB (Muta et al., 2003) and thus its expression will temper the immune activation. The *CBLB* product is required for the CD28 dependence of T-cell activation (Chiang et al., 2000). CD200 needs to be under tight regulation because while important for restraining immune responses (Minas and Liversidge, 2006) it also can promote tumorgenesis when overexpressed (Li et al., 2016; Miao et al., 2016). BTLA requires similar regulation because it relays immunosuppressant signalling and also polymorphisms in this gene are associated with increased cancer risk and autoimmune disease (Partyka et al., 2016; Shang et al., 2012). Thus in all cases the tighter regulation from adding spatial control would be required for these genes in the resting cells. Moreover, the retention of peripheral contacts for the adjacent LADs maintains these genes close to the periphery to potentially facilitate their rapid recruitment back to the periphery as needed to modulate the immune response as the initial T-cell activation dissipates.

Topological regulation of gene expression

Though to date there has been little overlap between the DamID and chromosome conformation capture literatures, this study demonstrates the importance of fusing these literatures to not only understand how the genome is configured but also how it is regulated. The clear separation of the lymphocyte enhancer and target genes while in LADs at the periphery is more interesting in light of a recent study showing that peripheral recruitment does not silence in of itself, but enhances the repression already initiated by transcriptional regulators induced with differentiation (Robson et al., 2016). Hence, rather than just placing the enhancer in a more transcriptionally permissive environment, the higher order

compartmental organization achieved here following peripheral release likely only influences gene regulation in context of the available transcription factors and their localized concentration at the newly created compartment.

In the case of lymphocyte activation what controls the initial tethering and release of these genes and enhancers is not yet clear. The restriction of so-regulated genes to those important for lymphocyte activation and the relatively small number of genes so regulated argues that their anchoring at the nuclear periphery is through a specific tether as opposed to general heterochromatin interactions. Such tethers have been previously described as nuclear envelope transmembrane proteins (NETs): liver-specific NET45 and NET47 contribute to liver-specific positioning of human chromosome 5 (Zuleger et al., 2013) and muscle-specific NETs Tmem38A, WFS1 and NET39 each contribute to changes during myogenesis in the positioning of largely non-overlapping subsets of genes important for muscle differentiation (Robson et al., 2016). More work will be required to ascertain the specific molecular tethers in this case. However, the release from the periphery could be as simple as transcriptional activation. Crispr/Cas9 targeting of either a DNA-binding VP16 domain capable of unfolding chromatin or a transcriptional activator was sufficient to release the *Ptn* locus from the periphery in one study (Therizols et al., 2014). The same activation could in theory apply to the enhancer identified here because activation of transcription from enhancers prior to their functional relevance has been reported (Arner et al., 2015).

While there is still much to be worked out, it is clear that in this case an enhancer induced during T-cell activation is released from the periphery along with several genes critical to T-cell regulation that are each in separate TADs to allow their interaction away from the nuclear envelope. While most characterized TADs isolate the enhancer and its gene target(s), these results indicate that lamina association can achieve the same functional isolation but enable a potentially much wider set of genes to be co-regulated by the enhancer across TAD boundaries. Hence, while the absolute number of enhancers released from the nuclear periphery concomitant with lymphocyte activation (Fig. 6) is not

large, the multiplicity of potential enhancer-gene pairings for each enhancer could allow this nuclear envelope regulation to influence a much larger set of genes.

Methods

Cell culture and transduction

Jurkat clone E6-1 T-cells and Raji B-cells were cultured in RPMI 1640 supplemented with 10% FBS, 100 units/ml penicillin and 100 µg/ml streptomycin. Jurkat and Raji cells were diluted 1:6 and 1:10, respectively, in fresh media every 2-3 days. Centrifugation at 1,000 rpm for 5 min was performed weekly during passaging to remove cellular debris. VSV-G pseudotyped lentivirus' encoding DamID, GFP-tagged, or pLKO constructs were generated as described in Supplemental Methods. 10 µg/ml protoamine sulphate was added during transduction to enhance efficiency.

Formation of immune conjugates with SEE-loaded Raji B-cells

Raji-B cells were incubated for 30 minutes at a concentration of 1 million cells/ml in RPMI 1640 media containing 0.5 µg/ml SEE (Toxin Technologies, Florida, EP404). Subsequently, SEE-loaded Raji cells were pelleted at 1,000 rpm for 5 min, washed twice in PBS by further centrifugation and then resuspended in suspension cell growth medium in 15 ml falcon tube. Conjugated Raji cells were then mixed in a 1:10 ratio with specified Jurkat cell lines to a total cell density of 1 million cells/ml in suspension cell growth medium. Samples were then extracted from mixed cultures at specified times for RNA extraction or fixation. For incubations longer than 1 hour, tube lids were loosened to allow gas exchange between cells within the tube and the incubator.

Fluorescence *In Situ* Hybridization (FISH)

For FISH experiments C2C12 MBs and MTs were cultured on coverslips and fixed in 4% paraformaldehyde (PFA), 1X PBS. FISH was performed as described in (Zuleger et al., 2013). Briefly, cells were permeabilized, cleared of RNA by RNase A and dehydrated with an ethanol series. DNA was denatured and captured in this state by a second ice-cold ethanol dehydration series. Coverslips were then annealed overnight to labelled BAC or whole chromosome probes. After washing probes were visualized with Alexafluor-conjugated Streptavidin/anti-digoxigenin antibodies and total DNA visualized with DAPI. To identify overexpressing cells, they were stained with GFP antibodies before FISH. Coverslips were mounted in Vectashield (Vector Labs), images of nuclear midplanes acquired and chromosome and gene positions determined using a macro run in Image Pro Plus. This measures nuclear area from DAPI images, divides the area into 5 shells of equal area through eroding 20% of total area in steps from the DAPI-defined nucleus, determines the shell containing the gene spot or the chromosome intensity per shell, and sums this for each cell.

Microarrays

RNA from Resting and Activated Jurkat T-cells was extracted with TRI-reagent (Invitrogen). After quality testing using an Agilent Bioanalyzer (RNA 6000 Nano total RNA kit, Agilent) the RNA was converted to biotin labelled-cRNA using the TotalPrep RNA Amplification Kit (Ambion, AMIL1791) following the manufacturer's instructions. The quality of cRNA was then confirmed again using the Agilent Bioanalyzer. Quality analysis and hybridization of the cRNA was performed at the Wellcome Trust Clinical Research Facility in Edinburgh. For each experiment, three biological replicates were hybridized to Illumina whole genome gene expression arrays (MouseWD6 BeadChip). Hybridizations were carried out using an Illumina Beadstation. The subsequent microarray data were quantile normalized using the free

statistics package R (R Development Core Team, 2010) using the Bioconductor package Limma (Smyth, 2005). Differentially expressed transcripts were selected with a log2 ratio above 0.5 in absolute value using moderated F-statistics adjusted for a false discovery rate of 5% (Benjamini and Hochberg, 1995).

DamID

DamID was performed as in (Vogel et al., 2007). Briefly, Resting Jurkat T-cells were transduced with Dam-Lamin B1- or Dam only-encoding lentiviruses over 24 h in the presence of 10ug/ul protamine sulphate. Transduced cells were then incubated with Raji B-cells ± SEE for a further 48 h after which genomic DNA was extracted and processed into libraries for next generation sequencing (Beijing Genomics). Sequenced reads were mapped to human Hg19 genome and the log2(Lamin B1/Dam) value determined for all genomic *DpnI* fragments in resting and activated cells, obtaining 2.2 and 2.1-fold genome coverage respectively. LADs were determined using a peak finder function in the BioConductor package DNAcopy, based in a circular binary segmentation algorithm (Seshan VE and Olshen A (2016). *DNAcopy: DNA copy number data analysis*. R package version 1.46.0). IP and PI regions were then identified as described previously (Robson et al., 2016) by comparing the mean intensity differences between Activated and Resting Jurkat T-cell log2(Lamin B1/Dam) values along running overlapping 100 kb windows. Regions with a mean Activated/Resting lamin B1 signal difference of 2 fold were then tested for significance against a randomized signal sample population using Fisher's exact test over 1,000 iterations. Regions with a P>0.01 were disregarded.

Supplemental information

Plasmids, antibodies, lentiviruses, bioinformatics, list of FISH probes and more detailed DamID and FISH procedures are described in Supplemental Methods.

4 Supplemental Figures, and Supplemental Methods.

Data access

DamID and gene expression datasets are currently being uploaded to GEO and will be publically available prior to publication.

Acknowledgements

We would like to thank Drs Czapiewski and Meinke for critical reading of the manuscript, Mr Lior Pytowski for assistance with taking images, Dr David Kelly for microscopy support, and Louise Evenden at the Wellcome Trust Clinical Research Facility for microarray analysis. MIR was supported by a Wellcome Trust PhD Studentship and funding for this work was provided by Wellcome Trust grants 095209 to ECS and 092076 for the Centre for Cell Biology.

Author contributions

Conceived of study and designed experiments, MIR and ECS; performed experiments, MIR; analyzed data, MIR, JdlH and ARWK; wrote the paper, MIR and ECS.

Disclosure declaration

The authors declare no conflicts of interest.

References

Amendola, M., and van Steensel, B. (2015). Nuclear lamins are not required for lamina-associated domain organization in mouse embryonic stem cells. EMBO Rep *16*, 610-617.

Andrey, G., Montavon, T., Mascrez, B., Gonzalez, F., Noordermeer, D., Leleu, M., Trono, D., Spitz, F., and Duboule, D. (2013). A switch between topological domains underlies HoxD genes collinearity in mouse limbs. Science *340*, 1234167.

Arner, E., Daub, C.O., Vitting-Seerup, K., Andersson, R., Lilje, B., Drablos, F., Lennartsson, A., Ronnerblad, M., Hrydziuszko, O., Vitezic, M.*, et al.* (2015). Transcribed enhancers lead waves of coordinated transcription in transitioning mammalian cells. Science *347*, 1010-1014.

Benjamini, Y., and Hochberg, Y. (1995). Controlling the false discovery rate: a practical and powerful apporach to multiple testing. J Royal Statistical Soc Series B *57*, 289-300.

Bernstein, B.E., Stamatoyannopoulos, J.A., Costello, J.F., Ren, B., Milosavljevic, A., Meissner, A., Kellis, M., Marra, M.A., Beaudet, A.L., Ecker, J.R.*, et al.* (2010). The NIH Roadmap Epigenomics Mapping Consortium. Nat Biotechnol *28*, 1045-1048.

Best, J.A., Blair, D.A., Knell, J., Yang, E., Mayya, V., Doedens, A., Dustin, M.L., Goldrath, A.W., and Immunological Genome Project, C. (2013). Transcriptional insights into the CD8(+) T cell response to infection and memory T cell formation. Nat Immunol *14*, 404-412.

Chiang, Y.J., Kole, H.K., Brown, K., Naramura, M., Fukuhara, S., Hu, R.J., Jang, I.K., Gutkind, J.S., Shevach, E., and Gu, H. (2000). Cbl-b regulates the CD28 dependence of T-cell activation. Nature *403*, 216-220.

Chubb, J.R., Boyle, S., Perry, P., and Bickmore, W.A. (2002). Chromatin motion is constrained by association with nuclear compartments in human cells. Curr Biol *12*, 439-445.

Consortium, E.P. (2012). An integrated encyclopedia of DNA elements in the human genome. Nature *489*, 57-74.

Dekker, J., and Mirny, L. (2016). The 3D Genome as Moderator of Chromosomal Communication. Cell *164*, 1110-1121.

Dixon, J.R., Selvaraj, S., Yue, F., Kim, A., Li, Y., Shen, Y., Hu, M., Liu, J.S., and Ren, B. (2012). Topological domains in mammalian genomes identified by analysis of chromatin interactions. Nature *485*, 376-380.

Drings, P., and Sonnemann, E. (1974). Phytohemagglutinin-induced increase of euchromatin contents in human lymphocytes. Res Exp Med (Berl) *164*, 63-76.

Fraser, J., Ferrai, C., Chiariello, A.M., Schueler, M., Rito, T., Laudanno, G., Barbieri, M., Moore, B.L., Kraemer, D.C., Aitken, S.*, et al.* (2015). Hierarchical folding and reorganization of chromosomes are linked to transcriptional changes in cellular differentiation. Mol Syst Biol *11*, 852.

Gonzalez-Granado, J.M., Silvestre-Roig, C., Rocha-Perugini, V., Trigueros-Motos, L., Cibrian, D., Morlino, G., Blanco-Berrocal, M., Osorio, F.G., Freije, J.M., Lopez-Otin, C.*, et al.* (2014). Nuclear envelope lamin-A couples actin dynamics with immunological synapse architecture and T cell activation. Sci Signal *7*, ra37.

Harr, J.C., Luperchio, T.R., Wong, X., Cohen, E., Wheelan, S.J., and Reddy, K.L. (2015). Directed targeting of chromatin to the nuclear lamina is mediated by chromatin state and A-type lamins. J Cell Biol *208*, 33-52.

Hewitt, S.L., High, F.A., Reiner, S.L., Fisher, A.G., and Merkenschlager, M. (2004). Nuclear repositioning marks the selective exclusion of lineage-inappropriate transcription factor loci during T helper cell differentiation. Eur J Immunol *34*, 3604-3613.

Hirschhorn, R., Decsy, M.I., and Troll, W. (1971). The effect of PHA stimulation of human peripheral blood lymphocytes upon cellular content of euchromatin and heterochromatin. Cell Immunol *2*, 696-701.

Hnisz, D., Abraham, B.J., Lee, T.I., Lau, A., Saint-Andre, V., Sigova, A.A., Hoke, H.A., and Young, R.A. (2013). Super-enhancers in the control of cell identity and disease. Cell *155*, 934-947.

Hnisz, D., Weintraub, A.S., Day, D.S., Valton, A.L., Bak, R.O., Li, C.H., Goldmann, J., Lajoie, B.R., Fan, Z.P., Sigova, A.A.*, et al.* (2016). Activation of proto-oncogenes by disruption of chromosome neighborhoods. Science *351*, 1454-1458.

Hou, C., Li, L., Qin, Z.S., and Corces, V.G. (2012). Gene density, transcription, and insulators contribute to the partition of the Drosophila genome into physical domains. Mol Cell *48*, 471-484.

Kind, J., Pagie, L., de Vries, S.S., Nahidiazar, L., Dey, S.S., Bienko, M., Zhan, Y., Lajoie, B., de Graaf, C.A., Amendola, M.*, et al.* (2015). Genome-wide maps of nuclear lamina interactions in single human cells. Cell *163*, 134-147.

Kind, J., Pagie, L., Ortabozkoyun, H., Boyle, S., de Vries, S.S., Janssen, H., Amendola, M., Nolen, L.D., Bickmore, W.A., and van Steensel, B. (2013). Single-cell dynamics of genome-nuclear lamina interactions. Cell *153*, 178-192.

Kind, J., and van Steensel, B. (2014). Stochastic genome-nuclear lamina interactions: modulating roles of Lamin A and BAF. Nucleus *5*, 124-130.

Korfali, N., Wilkie, G.S., Swanson, S.K., Srsen, V., Batrakou, D.G., Fairley, E.A., Malik, P., Zuleger, N., Goncharevich, A., de Las Heras, J.*, et al.* (2010). The leukocyte nuclear envelope proteome varies with cell activation and contains novel transmembrane proteins that affect genome architecture. Mol Cell Proteomics *9*, 2571-2585.

Kosak, S.T., Skok, J.A., Medina, K.L., Riblet, R., Le Beau, M.M., Fisher, A.G., and Singh, H. (2002). Subnuclear compartmentalization of immunoglobulin loci during lymphocyte development. Science *296*, 158-162.

Li, L., Tian, Y., Shi, C., Zhang, H., and Zhou, Z. (2016). Over-Expression of CD200 Predicts Poor Prognosis in Cutaneous Squamous Cell Carcinoma. Med Sci Monit *22*, 1079-1084.

Lupianez, D.G., Kraft, K., Heinrich, V., Krawitz, P., Brancati, F., Klopocki, E., Horn, D., Kayserili, H., Opitz, J.M., Laxova, R.*, et al.* (2015). Disruptions of topological chromatin domains cause pathogenic rewiring of gene-enhancer interactions. Cell *161*, 1012-1025.

Manteifel, V.M., Andreichuk, T.N., and Karu, T.I. (1992). A comparative study of chromatin from lymphocyte nuclei upon activation of transcription by irradiation from an He-Ne-laser or phytohemagglutinin. Mol Biol (Mosk) *26*, 1054-1062.

Meuleman, W., Peric-Hupkes, D., Kind, J., Beaudry, J.B., Pagie, L., Kellis, M., Reinders, M., Wessels, L., and van Steensel, B. (2013). Constitutive nuclear lamina-genome interactions are highly conserved and associated with A/T-rich sequence. Genome Res *23*, 270-280.

Miao, Y., Fan, L., Wu, Y.J., Xia, Y., Qiao, C., Wang, Y., Wang, L., Hong, M., Zhu, H.Y., Xu, W.*, et al.* (2016). Low expression of CD200 predicts shorter time-to-treatment in chronic lymphocytic leukemia. Oncotarget *7*, 13551-13562.

Minas, K., and Liversidge, J. (2006). Is the CD200/CD200 receptor interaction more than just a myeloid cell inhibitory signal? Crit Rev Immunol *26*, 213-230.

Muta, T., Yamazaki, S., Eto, A., Motoyama, M., and Takeshige, K. (2003). IkappaB-zeta, a new anti-inflammatory nuclear protein induced by lipopolysaccharide, is a negative regulator for nuclear factor-kappaB. J Endotoxin Res *9*, 187-191.

Neems, D.S., Garza-Gongora, A.G., Smith, E.D., and Kosak, S.T. (2016). Topologically associated domains enriched for lineage-specific genes reveal expression-dependent nuclear topologies during myogenesis. Proc Natl Acad Sci U S A *113*, E1691-1700.

Nora, E.P., Lajoie, B.R., Schulz, E.G., Giorgetti, L., Okamoto, I., Servant, N., Piolot, T., van Berkum, N.L., Meisig, J., Sedat, J.*, et al.* (2012). Spatial partitioning of the regulatory landscape of the X-inactivation centre. Nature *485*, 381-385.

Partyka, A., Tupikowski, K., Kolodziej, A., Zdrojowy, R., Halon, A., Malkiewicz, B., Dembowski, J., Frydecka, I., and Karabon, L. (2016). Association of 3' nearby gene BTLA polymorphisms with the risk of renal cell carcinoma in the Polish population. Urol Oncol. pii: S1078-1439(16)30044-8.

Peric-Hupkes, D., Meuleman, W., Pagie, L., Bruggeman, S.W., Solovei, I., Brugman, W., Graf, S., Flicek, P., Kerkhoven, R.M., van Lohuizen, M.*, et al.* (2010). Molecular maps of the reorganization of genome-nuclear lamina interactions during differentiation. Mol Cell *38*, 603-613.

Pickersgill, H., Kalverda, B., de Wit, E., Talhout, W., Fornerod, M., and van Steensel, B. (2006). Characterization of the Drosophila melanogaster genome at the nuclear lamina. Nat Genet *38*, 1005-1014.

Pindyurin, A.V., Moorman, C., de Wit, E., Belyakin, S.N., Belyaeva, E.S., Christophides, G.K., Kafatos, F.C., van Steensel, B., and Zhimulev, I.F. (2007). SUUR joins separate subsets of PcG, HP1 and B-type lamin targets in Drosophila. J Cell Sci *120*, 2344-2351.

Plank, J.L., and Dean, A. (2014). Enhancer function: mechanistic and genome-wide insights come together. Mol Cell *55*, 5-14.

Pompidou, A., Rousset, S., Mace, B., Michel, P., Esnous, D., and Renard, N. (1984). Chromatin structure and nucleic acid synthesis in human lymphocyte activation by phytohemagglutinin. Exp Cell Res *150*, 213-225.

Rao, S.S., Huntley, M.H., Durand, N.C., Stamenova, E.K., Bochkov, I.D., Robinson, J.T., Sanborn, A.L., Machol, I., Omer, A.D., Lander, E.S.*, et al.* (2014). A 3D map of the human genome at kilobase resolution reveals principles of chromatin looping. Cell *159*, 1665-1680.

Rawlings, J.S., Gatzka, M., Thomas, P.G., and Ihle, J.N. (2011). Chromatin condensation via the condensin II complex is required for peripheral T-cell quiescence. EMBO J *30*, 263-276.

Robson, M.I., de Las Heras, J.I., Czapiewski, R., Le Thanh, P., Booth, D.G., Kelly, D.A., Webb, S., Kerr, A.R., and Schirmer, E.C. (2016). Tissue-Specific Gene Repositioning by Muscle Nuclear Membrane Proteins Enhances Repression of Critical Developmental Genes during Myogenesis. Mol Cell *62*, 834-847.

Sanyal, A., Lajoie, B.R., Jain, G., and Dekker, J. (2012). The long-range interaction landscape of gene promoters. Nature *489*, 109-113.

Schoenfelder, S., Furlan-Magaril, M., Mifsud, B., Tavares-Cadete, F., Sugar, R., Javierre, B.M., Nagano, T., Katsman, Y., Sakthidevi, M., Wingett, S.W.*, et al.* (2015). The pluripotent regulatory circuitry connecting promoters to their long-range interacting elements. Genome Res *25*, 582-597.

Schoenfelder, S., Sexton, T., Chakalova, L., Cope, N.F., Horton, A., Andrews, S., Kurukuti, S., Mitchell, J.A., Umlauf, D., Dimitrova, D.S.*, et al.* (2010). Preferential associations between co-regulated genes reveal a transcriptional interactome in erythroid cells. Nat Genet *42*, 53-61.

Sexton, T., Yaffe, E., Kenigsberg, E., Bantignies, F., Leblanc, B., Hoichman, M., Parrinello, H., Tanay, A., and Cavalli, G. (2012). Three-dimensional folding and functional organization principles of the Drosophila genome. Cell *148*, 458-472.

Shang, Y., Guo, G., Cui, Q., Li, J., Ruan, Z., and Chen, Y. (2012). The expression and anatomical distribution of BTLA and its ligand HVEM in rheumatoid synovium. Inflammation *35*, 1102-1112.

Shen, Y., Yue, F., McCleary, D.F., Ye, Z., Edsall, L., Kuan, S., Wagner, U., Dixon, J., Lee, L., Lobanenkov, V.V.*, et al.* (2012). A map of the cis-regulatory sequences in the mouse genome. Nature *488*, 116-120.

Smyth, G.K. (2005). Limma: linear models for microarray data. In Bioinformatics and Computational Biology Solutions Using R and Bioconductor, R. Gentleman, V. Carey, S. Dudoit, R. Irizarry, and W. Huber, eds. (New York: Springer), pp. 397-420.

Strickfaden, H., Zunhammer, A., van Koningsbruggen, S., Kohler, D., and Cremer, T. (2010). 4D chromatin dynamics in cycling cells: Theodor Boveri's hypotheses revisited. Nucleus *1*, 284-297.

Therizols, P., Illingworth, R.S., Courilleau, C., Boyle, S., Wood, A.J., and Bickmore, W.A. (2014). Chromatin decondensation is sufficient to alter nuclear organization in embryonic stem cells. Science *346*, 1238-1242.

Vogel, M.J., Peric-Hupkes, D., and van Steensel, B. (2007). Detection of in vivo protein-DNA interactions using DamID in mammalian cells. Nat Protoc *2*, 1467-1478.

Zuleger, N., Boyle, S., Kelly, D.A., de Las Heras, J.I., Lazou, V., Korfali, N., Batrakou, D.G., Randles, K.N., Morris, G.E., Harrison, D.J.*, et al.* (2013). Specific nuclear envelope transmembrane proteins can promote the location of chromosomes to and from the nuclear periphery. Genome Biol *14*, R14.

Figures and Legends

Figure 1

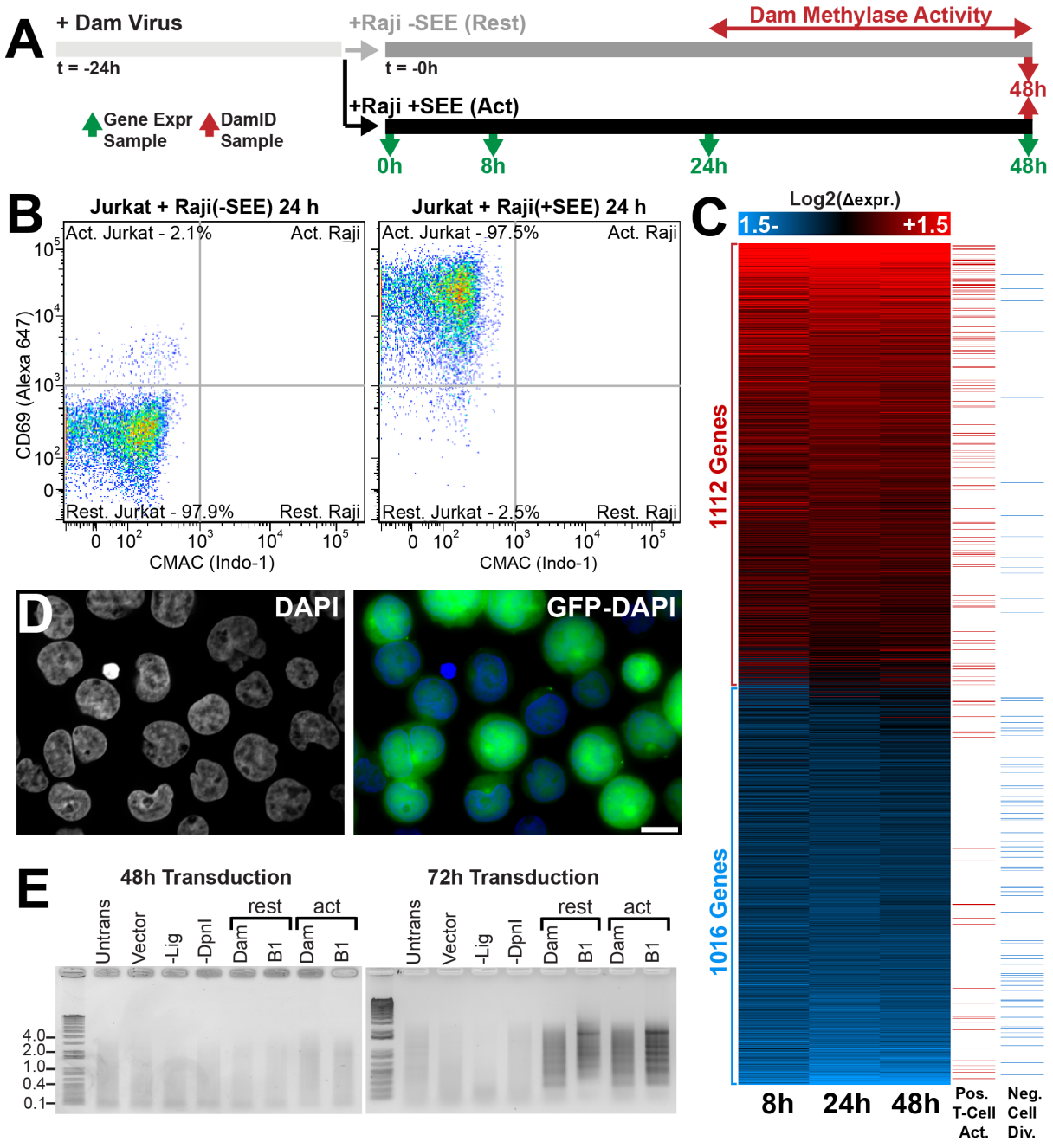

Figure 1. Determination of Gene Expression and Genome Organisational Changes during T-cell Activation. (*A*) Schematic diagram demonstrating methodology for microarray gene expression and DamID analysis of Resting and Activated Jurkat T-cells. (*B*) FACs plot of CD69 vs CMAC staining for Resting and Activated Jurkat T-cells. Raji B-cells were previously stained with CMAC to distinguish the antigen presenting cell from Jurkat T-cells. 97.5% of Jurkat T-cells become activated when stimulated with SEE conjugated Raji B-cells. (*C*) Heat map of gene expression changes of at least 1.4 fold with GO terms associated with positive regulation of T-cell activation or negative regulation of cell division. (*D*) Representative micrograph of Jurkat T-cells transduced with

a GFP-encoding lentivirus. E. Agarose gels of PCR amplified Dam methylated genomic DNA. Amplification is only observed in Resting or Activated cells 72 h post transduction. T4 DNA ligase null (-Lig) and *DpnI* null (-*DpnI*) controls represent background amplification. See also Fig. S1.

Figure 2

A

Sample	% of Genome	Number	Median Size (Kbp)	Min. Size (Kbp)	Max. Size (Mbp)	# Genes
Rest. LADs	41.3%	2,075	236	50	10.6	3477

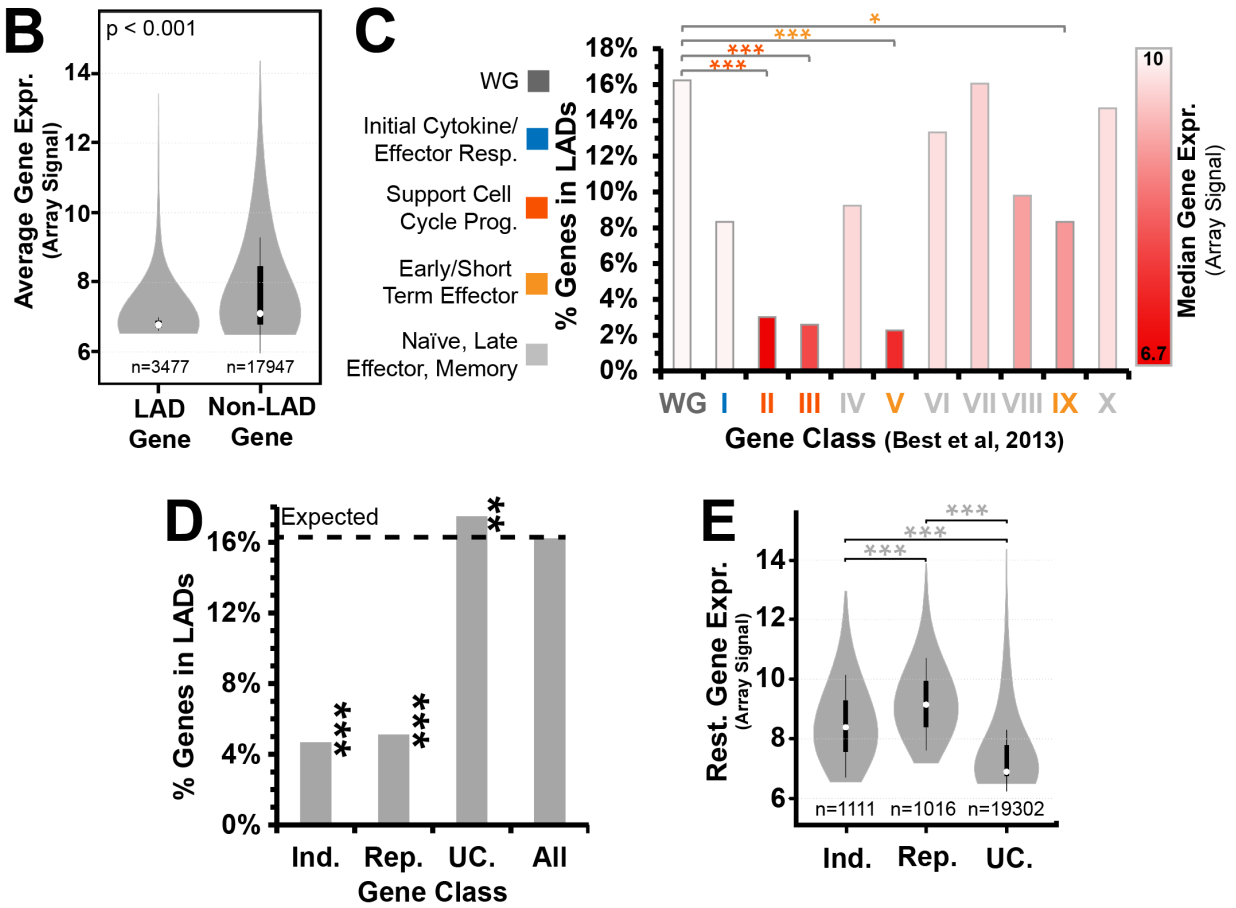

Figure 2. A The genome of resting T-cells is partially pre-configured for T-cell activation. (*A*) Table summarizing parameters of identified resting LADs. (*B*) Violin plot showing the microarray determined gene expression level of genes within LADs is less than genes within non-LAD regions. (*C*) Summary of the gene expression and fraction with lamina-association of 10 categories of genes displaying distinct transcriptional behaviours during T-cell activation (Best et al., 2013). Classes associated with early effector function and cell division are more expressed and less frequently in LADs than classes associated with late effector/memory function. Further details of classes can be found in Figure S1. (*D*) Bar plot indicating genes induced or repressed at least 1.4 fold during T-cell activation are 4 times less frequently found in LADs than the whole genome in resting Jurkat T-cells. (*E*) Violin plot demonstrating induced or repressed genes are also more highly expressed than the whole genome in resting Jurkat T-cells. For B and E, significance of difference in microarray gene expression was determined by Kolmogorov-Smirnov (KS) test. For C and D statistical significance was determined by χ^2 tests. *P < 0.05, **P < 0.01 and *** P < 0.001. See also Fig. S2.

Figure 3

A

Sample	% of Genome	Number	Median Size (Kbp)	Min. Size (Kbp)	Max. Size (Mbp)	# Genes
Rest. LADs	41.3%	2,075	236	50	10.6	3477
Act. LADs	40.5%	2,174	215	50	10.6	3275
IP Regions	2.1%	1070	52	25	274.6	156
PI Regions	3.5%	2969	47	25	328.8	799

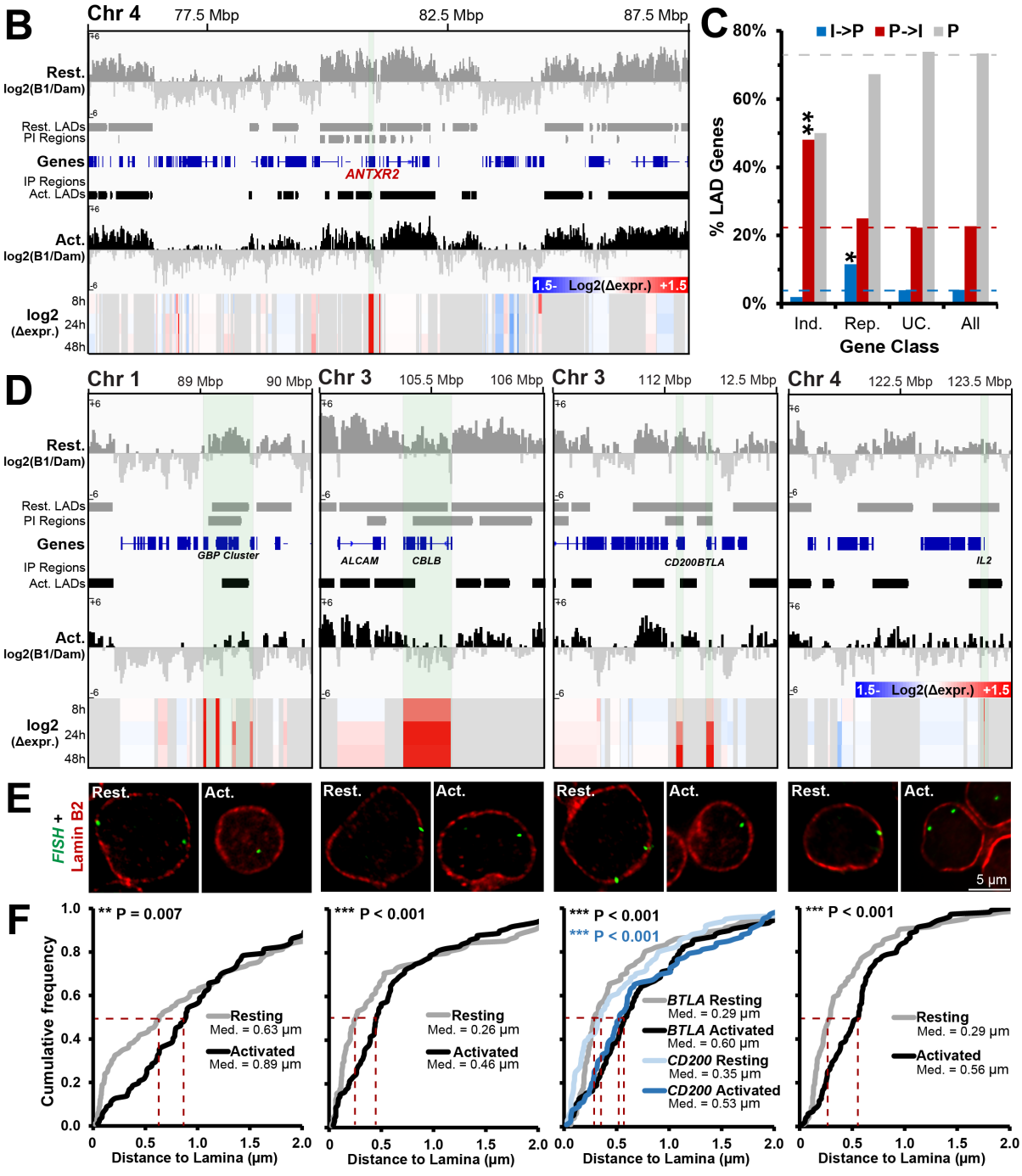

Figure 3. A Number of Critical Genes are Released from the Periphery during T-cell Activation. (*A*) Table summarizing parameters of identified LADs and regions showing increased (IP) and decreased (PI) association with the nuclear periphery between resting and activated Jurkat T-cells. (*B*) Genome browser view for the genomic region surrounding *ANTRX2* showing DamID signal intensities, identified LADs, IP and PI regions and microarray gene expression changes for Resting and Activated Jurkat T-cells. (*C*) Bar plot demonstrating the DamID behaviours of genes found

within LADs in resting Jurkat T-cells. 50% genes found in LADs in resting cells that are induced during activation concomitantly display decreased peripheral association. Statistical significance was determined by χ^2 tests. *P < 0.05, **P < 0.01 and *** P < 0.001. (*D*) Genome browser views for the genomic region surrounding the GBP gene cluster and *CBLB, CD200, BTLA* and *IL2* loci. DamID signal intensities, identified LADs, IP and PI regions and microarray gene expression changes for Resting and Activated Jurkat T-cells are shown. (*E,F*) Representative micrographs and quantification of gene positions in resting and activated cells relative to lamin B2. For quantification statistics, the position of loci in the activated sample was compared to the resting sample by KS tests. *P < 0.05, **P < 0.01 and *** P < 0.001. See also Fig. S2.

Figure 4

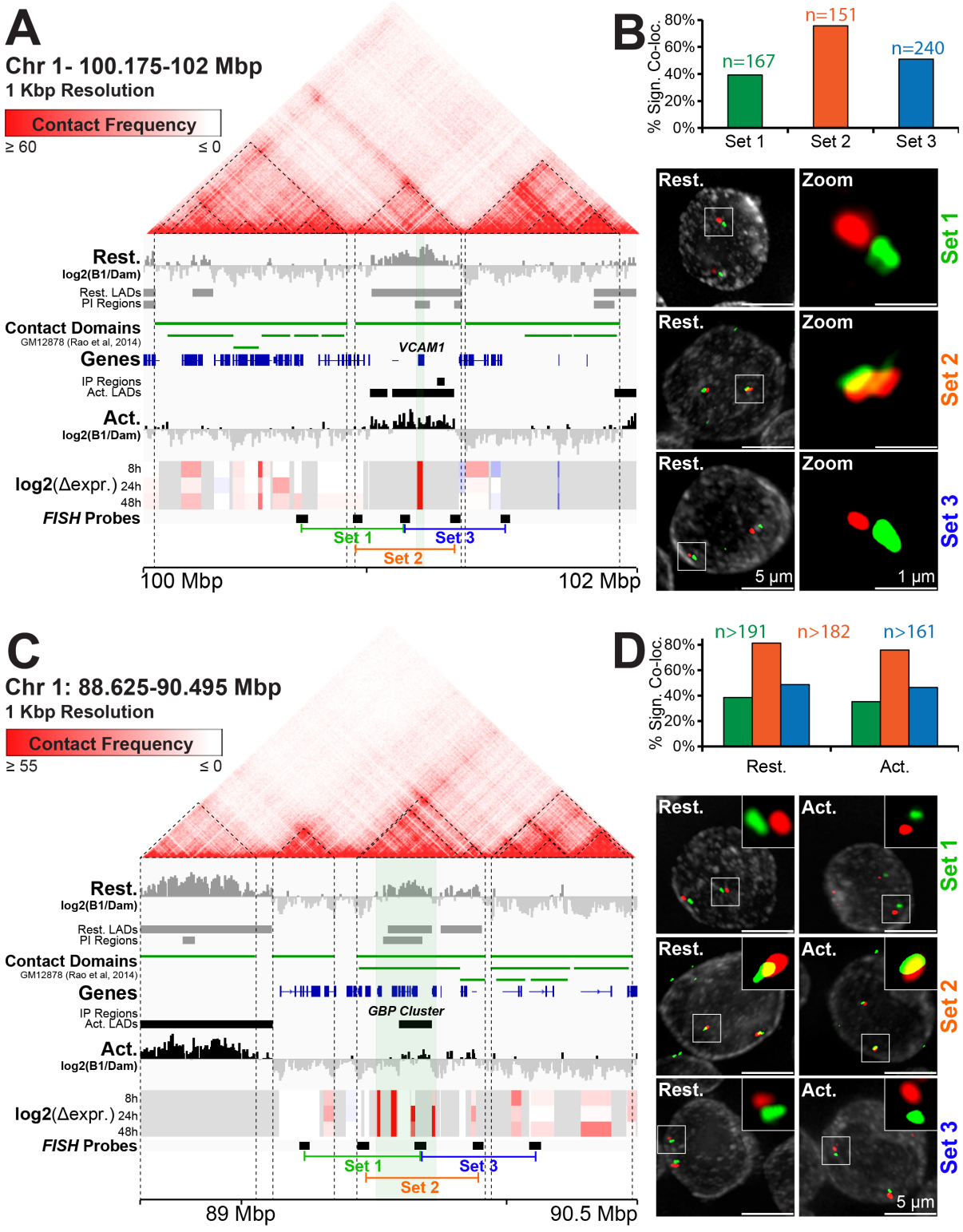

Figure 4. The Unit of Repositioning is the TAD. (*A*) Genome browser view for the genomic region surrounding *VCAM1* showing Hi-C data and associated Contact Domains (dotted lines) determined in GM12878 lymphoblastoid cells (Rao et al., 2014). DamID signal intensities, identified LADs, IP and PI regions and microarray gene expression changes for resting and activated Jurkat T-cells are shown below. (*B*) Quantification and representative max projection images displaying distance between indicated sets of ~150 kbp spaced FISH probe pairs. Set 1 and 3, containing probe

pairings from different TADs, display significant co-localisation less frequently than probes within the same TAD used for Set 2. (*C*) Identical genome browser view of the GBP gene cluster. (*D*) Quantification and representative images displaying distance between indicated sets of ~175 kbp spaced FISH probe pairs in resting and activated Jurkat T-cells. The degree of co-localisation is unchanged for all probe pairs indicating the TAD structure is pre-established when at the nuclear periphery.

Figure 5

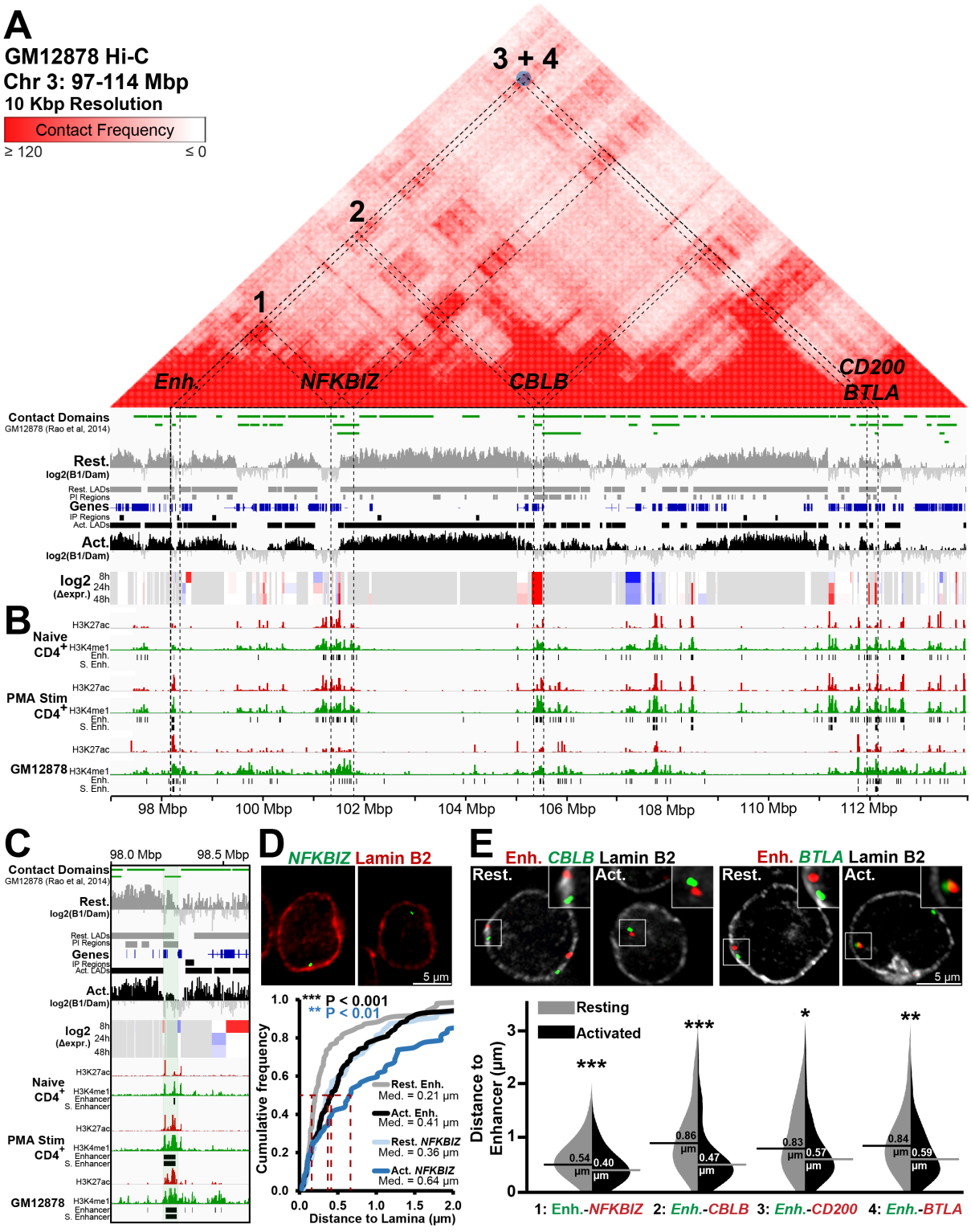

Figure 5. Peripheral Positioning Prevents Enhancer Association with Target Genes in Resting T-cells. (*A*) Genome browser view of a 17 Mbp region of chromosome 3 with GM12878 cell Hi-C interactions (Rao et al., 2014) and Contact Domains, DamID signal intensities, identified LADs, IP and PI regions and microarray gene expression changes for Resting and Activated Jurkat T-cells displayed. Blue dot represents highly significant DNA-DNA contacted detected by Rao, et al. (*B*)

Parallel views of published H3K27ac and H3K4me1 Chip-seq tracks in Naïve and PMA-stimulated $CD4^+$ T-cells (Bernstein et al., 2010) and GM12878 lymphoblastoid cells ((Consortium, 2012); ENCODE) with H3K27ac-defined Enhancers (Enh.) and so called super enhancers (S. Enh) labelled (Hnisz et al., 2013). Several genes, *NFKBIZ, CBLB, CD200* and *BTLA,* and a T-cell activation-specific enhancer (Enh.), display reduced lamina-association during T-cell activation concomitant with transcriptional induction and display long range Hi-C interactions in GM12878 cells. (*C*) Zoomed genome browser view of the Enhancer region. (*D*) Representative micrographs and quantification of enhancer and *NFKBIZ* positions in resting and activated cells relative to lamin B2. (*E*) Violin plot quantification and representative images of distances between the enhancer and indicated genes in resting and activated cells. All enhancer-gene FISH probe combinations display reduced inter-probe distance following activation. See also Figure S3.

Figure 6

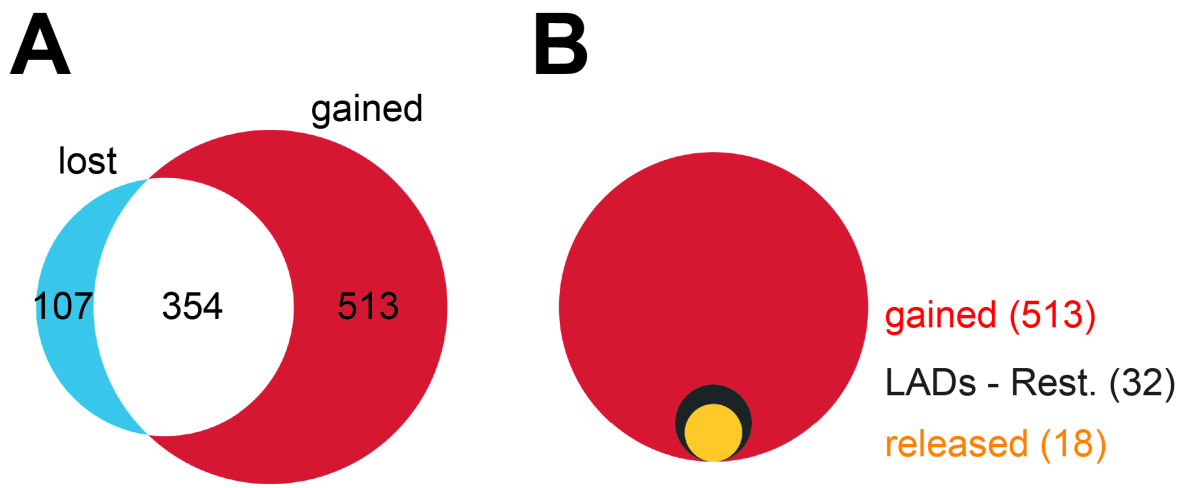

Figure 6. Enhancers are Released from the Periphery during T-cell Activation. (*A*) Upon lymphoblast activation, ~50% of the total number of enhancers described in this system are induced (red), while only 10% were silenced (blue). (*B*) Of the 513 enhancers that are induced upon activation, most are located in interLAD regions. Of the 32 enhancers that were associated with LADs in the resting state, more than half become released upon lymphoblast activation.

Supplemental information

Lymphocyte genes and an enhancer sequestered at the nuclear periphery undergo constrained release and associate upon T-cell activation

Michael I. Robson, Jose I. de las Heras, Alastair R. W. Kerr

and Eric C. Schirmer

Supplemental Methods

Supplemental References

Supplemental Figures

Supplemental methods

Plasmid and cell sources

psPAX2 and pMD2.G were a gift from Justina Cholewa-Waclaw (Adrian Bird, WTCCB, Edinburgh). pLgw Dam-V5-Lamin B1 and pLgw V5-Dam were a gift from the van Steensel laboratory. Jurkat T-lymphocyte clone E6-1 was purchased from ATCC while Raji lymphoblastoid cells were a gift from Professor Vicente Andrés (Centro Nacional de Investigaciones Cardiovasculares. Madrid, Spain).

Antibodies

Rabbit anti-Lamin B2 (Schirmer et al., 2001) and anti-GFP (Invitrogen) antibodies was used at a 1:400 and 1:200 dilution, respectively. For visualization of primary antibodies for immunofluorescence, donkey anti-rabbit pig secondary antibodies conjugated to a variety of Alexa Fluor® dyes were used (Molecular Probes, Invitrogen). For the detection of biotin- or digoxigenin-labelled probes in FISH experiments, streptavidin (Molecular Probes, Invitrogen) or anti-digoxigenin antibodies (Jackson labs) conjugated to Alexa Fluor® dyes were used, respectively.

Lentivirus generation and transduction

Lentiviruses encoding DamID constructs were generated as described in (Salmon and Trono, 2007) with several modifications. Briefly, non-replicative lentiviruses were generated by transfection of ~6 million 293FT cells plated in a 8.5 cm diameter tissue culture plate with 2.8 μg pMD2.G, 4.6 μg psPAX2 and 7.5 μg of the construct-specific transfer vector using 36 μl lipofectamine 2000 in 3 ml Optimem as per the manufacturer's instructions. After 16 h

293FT media was replaced. 48 h later the virus containing supernatant was aspirated, cleared of cellular debris by centrifugation for 10 min at 3,500 rpm and followed by filtration through a 0.45 μm^2 low protein binding PES syringe filter (Millipore, SLHP003RS). Viruses were then concentrated by ultracentrifugation at 55,000 x *g* for 75 min at 4^{o}C in a JA-25.5 rotor and resuspended in an appropriate volume of Opti-MEM. If not used immediately, aliquots were frozen at -80°C. Transduction was performed in the presence of 10 μg/ml protoamine sulphate.

Bioinformatics

Genes differentially expressed in resting and activated Jurkat T-cells analyzed for Biological Process and Cellular Compartment GO-term enrichment using Gene Ontology enrichment analysis and visualization tool GOrilla (Eden et al., 2009). Genes upregulated during T-cell activation were significantly enrichment in terms positively associated with T-cell activation while those downregulated were enriched in terms associated with negative regulation of the cell cycle. A full list of GO-terms enriched in genes upregulated and downregulated during T-cell activation can be found in Supplementary Figure S1. To demonstrate the gene expression changes associated with GO-categories, specific GO-terms that either support T-cell activation or negatively regulate cell cycle were selected and displayed in Fig. 1. These terms are shown in Fig. S1.

In order to accurately compare the overlap between LADs and TADS in both resting and activated cells, we down-sampled the number of LADs in each file randomly to 500 features and counted the number of times a LAD was found completely within a TAD. We then randomised the location of each LAD per chromosome in the down-sampled files and counted the number of overlaps to TADs. This process was repeated 1000 times in order view the distribution of overlaps in randomised and non-randomised LAD/TAD overlaps. Both the scripts and the data used for figure S3 can be retrieved from the github

site: https://github.com/AlastairKerr/Robson2016). No statistics are given because a non-overlapping distribution will always have a p-value near 0.

DamID (more detailed)

DamID was performed as described in (Vogel et al., 2007). Briefly for each DamID sample two million Jurkat cells were transduced with $^{1}/_{10}$ of a Dam methylase encoding lentiviral preparation in the presence of 10 µg/ml protamine sulphate in a 3.5 cm diameter tissue culture dish. After 24 h cells were pelleted at 200 x *g* for 4 min and resuspended in fresh suspension cell growth media. Dam-control or Dam-Lamin B1-transduced Jurkat T-cells were then incubated with untransduced Raji B cells ±SEE and left a further 48 h, diluting cells in appropriate volumes of suspension cell growth media to sustain logarithmic growth, before proceeding with DNA extraction.

DamID sample processing was then performed as described in Vogel et al. Briefly, DNA was extracted from cells using the DNeasy tissue lysis kit (Qiagen) as per manufacturer's instructions. 2.5 µg of extracted DNA was then digested by *DpnI* (NEB) and, following heat inactivation of *DpnI,* was ligated to the DamID adaptor duplex (dsAdR) generated from the oligonucleotides AdRt (5'-CTAATACGACTCACATAGGGCAGCGTGGTCGCGGCCGA-GGA-3') and AdRb (5'-TCCTCGGCCG-3') after which DNA was further digested by *DpnII*. To amplify DNA sequences methylated by the Dam methylase, 5 µl of *DpnII* digested material was then subjected to PCR in the supplied buffer in the presence of the 1.25 µM Adr-PCR primer (5'-GGTCGCGGCCGAGGATC-3'), 0.2 mM dNTPs and 1X of the Advantage cDNA polymerase (Clontech, cat. no. 639105). PCR was performed as described in table below.

PCR program for DNA amplification in DamID.

Cycle	Denature	Anneal	Extend
1			68°C for 10 min
2	94°C for 3 min	65°C for 5 min	68°C for 15 min
3-6	94°C for 1 min	65°C for 1 min	68°C for 10 min
7-23	94°C for 1 min	65°C for 1 min	68°C for 2 min

Following PCR, the distribution of amplified DNA fragments was checked on agarose gels (Fig. 1). If samples were of sufficient quality DNA was purified on QIAquick PCR purification columns (Qiagen) and then concentrated to the required concentration by precipitation. To generate the 2 µg of material required of next generation sequencing it was found an average of 6-8 PCR reactions were required per sample.

DamID Sequencing and Analysis

DamID sample libraries were prepared for next generation sequencing by fragmentation followed by ligation to sequencing adaptors. Libraries were then sequenced by 90 bp paired end (90PE) sequencing in reactions with 5 samples per well. DamID sequences were aligned to the human Hg19 genome using the Burrows-Wheeler Aligner software bwa-mem (Li and Durbin, 2009). Subsequent processing was performed using R (R Core Team (2015). R: A language and environment for statistical computing. R Foundation for Statistical Computing, Vienna, Austria. URL https://www.R-project.org/) and Bedtools (Quinlan and Hall, 2010). Resting and Activated Jurkat DamID data was quantified at a *DpnI* fragment level by counting the number of reads that overlapped each *DpnI*-flanked (GATC) genomic fragment for each pair of Dam-alone and Dam-LaminB1 samples. The log2 ratios between Dam-LaminB1 and Dam-alone were calculated for each DpnI fragment, and the resulting values quantile normalized in R using the BioConductor Limma package (Ritchie et al., 2015) to allow a more quantifiable sample comparison.

Lamina Associated Domains (LADs) Definition

To identify LADs we used a circular binary segmentation algorithm in the Bioconductor package DNAcopy (Seshan VE and Olshen A (2016). *DNAcopy: DNA copy number data analysis*. R package version 1.46.0) using the default parameters. The positive signal tracts were extracted and merged if they were <8Kb apart. To reduce the noise from low signal low level LADs, we removed anything below 50Kb from our LAD list. This threshold was chosen empirically after careful examination of the LAD traces. We considered a gene being in a LAD if it overlapped with one.

Identification of Genomic Regions with Altered Peripheral Association

To identify genomic regions with differential frequencies of association with the periphery in resting vs activating lymphoblasts, a statistical test was devised and described in (Robson et al., 2016). A moving window of 45 *DpnI* fragments (~25Kb) were run along each chromosome, with a shift of 10 *DpnI* fragments (~5Kb). From this the average DamID signal the difference between resting and activated lymphoblasts was calculated within each window. Windows with a signal difference greater than 2-fold were flagged as potential differential regions. These regions were then tested for statistical significance compared to a shuffled sample (x1,000 iterations) using Fisher's exact test. The regions that passed with $p<0.01$ were termed PI or IP regions, to denote regions that exhibited a significant repositioning becoming to the interior (PI) or to the periphery (IP) during lymphocyte activation

Fluorescence *In Situ* Hybridization (more detailed)

For FISH experiments Resting and Activated Jurkat cells were pelleted at 200 x g for 5 min and resuspended in PBS. Cells were then plated onto poly-lysine coated coverslips, left for 5 minutes and then fixated in 4% para-formaldehyde, 1X PBS for 10 min at room temperature. After aging coverslips for several days, cells were permeabilized for 6 min with 0.2% Triton-X-100 in PBS, followed by 3 washes in PBS. If antibody staining was required coverslips were blocked with 1% BSA prior to sequential incubations with primary and secondary antibodies. After washing, antibodies were fixed for 45 s in 2% paraformaldehyde, PBS. Cells were next pre-equilibrated in 2X SCC and treated with RNase A (100µg/ml) at 37ºC for 1 h. Following washing in 2X SCC, cells were dehydrated with a 70%, 85% and 100% ethanol series. Coverslips were then air dried, heated to 70ºC and submerged into 85ºC preheated 70% formamide, 2X SSC (pH 7.0) for 21 min. A second ethanol dehydration series was then performed using -20ºC 70% ethanol for the first step. Coverslips were air dried and 150-300 ng biotin-/digoxigenin-/fluorophore-labelled probe was added in hybridization buffer (50% formamide, 2X SSC, 1% Tween20, 10% Dextran Sulphate) containing 6 µg human Cot1 DNA (Invitrogen) and sheared salmon sperm DNA and incubated at 37°C for 24 h in a humidified chamber. After incubation, the coverslips were washed four times for 3 min each in 2X SSC at 50ºC followed by four times for 3 min each in 0.1X SSC at 65ºC. Coverslips were then pre-equilibrated in 2X SSC, 0.1% Tween-20 and blocked with 4% BSA before incubating for 1 h at room temperature with Alexa Fluor®conjugated-Steptavidin/anti-dioxigenin antibodies and 4,6-diamidino-2 phenylindole, dihydrochloride (DAPI) at 2 µg/ml. Coverslips were subsequently washed 3 times in 2X SSC, 0.1% Tween-20 at 37ºC and mounted on slides in Vectashield (Vector Labs). BACs were ordered as indicated in the table below.

List of FISH probes.

Locus	BAC	Chr	Start	End
GBP 1	WI2-1164H23	1	89,225,254	89,263,381
GBP 2	WI2-1912I12	1	89,441,903	89,486,300
GBP 3	WI2-2752H5	1	89,657,420	89,702,009
GBP 4	WI2-526L3	1	89,876,247	89,917,750
GBP 5	WI2-1217K14	1	90,091,207	90,135,261
VCAM 1	WI2-2673A12	1	100,736,026	100,781,301
VCAM 2	WI2-1322N21	1	100,934,306	100,971,590
VCAM 3	WI2-1574P13	1	101,119,857	101,157,755
VCAM 4	WI2-569L23	1	101,303,334	101,342,416
VCAM 5	WI2-481B14	1	101,490,965	101,526,327
Enhancer	WI2-898A6	3	98,250,119	98,286,966
NFKBIZ	WI2-645D14	3	101,546,513	101,590,433
CBLB	WI2-628H6	3	105,507,827	105,545,557
BTLA	WI2-1965N10	3	112,175,307	112,212,883
CD200	WI2-526H19	3	112,039,557	112,083,246
IL-2	CH17-337H11	4	123,272,797	123,467,914
CD25	CH17-215L21	10	6,001,620	6,232,731

Determination of FISH-labelled Gene Position

The position of the loci and chromosomes was determined using previously designed macros written in Visual Basic and run on Image Pro Plus (available on request). Briefly, the macro calculates the DAPI-identified nuclear cross-sectional area and then sequentially erodes 20% of this in 4 stages to generate 5 shells of roughly equal area. The shell containing the locus was then determined and the number of events in each shell summed. The percentage of total events in each shell was then calculated in excel. Only cells that had the locus in focus at the mid-plane of the nucleus were analyzed.

Microscopy

Images were acquired on a Nikon TE-200 microscope using a 1.45 NA 100x objective, Sedat quad filter set, PIFOC Z-axis focus drive (Physik Instrubments) and a CoolSnapHQ

High Speed Monochrome CCD camera (Photometrics) run by Metamorph image acquisition software.

Supplemental references

Eden, E., Navon, R., Steinfeld, I., Lipson, D., and Yakhini, Z. (2009). GOrilla: a tool for discovery and visualization of enriched GO terms in ranked gene lists. BMC Bioinformatics *10*, 48.

Li, H., and Durbin, R. (2009). Fast and accurate short read alignment with Burrows-Wheeler transform. Bioinformatics *25*, 1754-1760.

Quinlan, A.R., and Hall, I.M. (2010). BEDTools: a flexible suite of utilities for comparing genomic features. Bioinformatics *26*, 841-842.

Ritchie, M.E., Phipson, B., Wu, D., Hu, Y., Law, C.W., Shi, W., and Smyth, G.K. (2015). limma powers differential expression analyses for RNA-sequencing and microarray studies. Nucleic acids research *43*, e47.

Robson, M.I., de Las Heras, J.I., Czapiewski, R., Le Thanh, P., Booth, D.G., Kelly, D.A., Webb, S., Kerr, A.R., and Schirmer, E.C. (2016). Tissue-Specific Gene Repositioning by Muscle Nuclear Membrane Proteins Enhances Repression of Critical Developmental Genes during Myogenesis. Molecular cell *62*, 834-847.

Salmon, P., and Trono, D. (2007). Production and titration of lentiviral vectors. Curr Protoc Hum Genet *Chapter 12*, Unit 12 10.

Schirmer, E.C., Guan, T., and Gerace, L. (2001). Involvement of the lamin rod domain in heterotypic lamin interactions important for nuclear organization. J Cell Biol *153*, 479-489.

Vogel, M.J., Peric-Hupkes, D., and van Steensel, B. (2007). Detection of in vivo protein-DNA interactions using DamID in mammalian cells. Nat Protoc *2*, 1467-1478.

Supplementary Figures

Figure S1

A Selected GO Terms Displayed in Figure 1B

Up Regulated Gene-Enriched

GO Term	Description	P-value	FDR q-value	Enrichment
GO:0032732	pos. reg. of interleukin-1 production	9.1E-04	2.6E-02	3.8
GO:2000406	pos. reg. of T cell migration	9.9E-04	2.8E-02	4.9
GO:0050729	pos. reg. of inflammatory response	8.5E-04	2.5E-02	2.4
GO:0045630	pos. reg. of T-helper 2 cell diff.	3.5E-04	1.2E-02	9.8
GO:0002830	pos. reg. of type 2 immune response	5.8E-04	1.8E-02	6.6
GO:0045624	pos. reg. of T-helper cell diff.	3.9E-04	1.3E-02	5.7
GO:0043372	pos. reg. of CD4-positive, alpha-beta T cell diff.	4.2E-05	1.8E-03	5.7
GO:2000403	pos. reg. of lymphocyte migration	5.6E-04	1.8E-02	4.6
GO:0001916	pos. reg. of T cell mediated cytotoxicity	1.9E-04	6.9E-03	6.4
GO:0001912	pos. reg. of leukocyte mediated cytotoxicity	1.6E-05	7.7E-04	5.0
GO:0002708	pos. reg. of lymphocyte mediated immunity	5.4E-08	5.0E-06	4.5
GO:0002705	pos. reg. of leukocyte mediated immunity	6.5E-08	6.0E-06	4.0
GO:0045621	pos. reg. of lymphocyte diff.	1.6E-06	9.9E-05	3.6
GO:0045582	pos. reg. of T cell diff.	5.9E-07	4.3E-05	4.1
GO:0043372	pos. reg. of CD4-positive, alpha-beta T cell diff.	4.2E-05	1.8E-03	5.7
GO:0045580	reg. of T cell diff.	9.8E-10	1.4E-07	4.0
GO:0002684	pos. reg. of immune system process	9.7E-26	4.6E-22	2.6
GO:0001817	reg. of cytokine production	1.2E-14	5.1E-12	2.5
GO:0002696	pos. reg. of leukocyte act.	1.5E-19	1.3E-16	3.7
GO:0050863	reg. of T cell act.	8.1E-20	9.6E-17	3.7
GO:2000516	pos. reg. of CD4-positive, alpha-beta T cell act.	1.4E-05	6.8E-04	5.7
GO:2000107	neg. reg. of leukocyte apoptotic process	2.6E-04	9.2E-03	3.7
GO:0051251	pos. reg. of lymphocyte act.	5.5E-19	4.3E-16	3.9
GO:0050671	pos. reg. of lymphocyte proliferation	2.1E-09	2.7E-07	3.7
GO:0042102	pos. reg. of T cell proliferation	2.6E-07	2.0E-05	3.7
GO:0050870	pos. reg. of T cell act.	1.8E-15	8.1E-13	3.9
GO:0031295	T cell costimulation	1.9E-08	2.0E-06	4.5
GO:0045084	pos. reg. of interleukin-12 biosynthetic process	3.5E-04	1.2E-02	9.8
GO:0050852	T cell receptor signaling pathway	2.5E-05	1.1E-03	2.7
GO:0060337	type I interferon signaling pathway	3.7E-14	1.2E-11	6.2
GO:0060333	interferon-gamma-mediated signaling pathway	4.0E-18	2.6E-15	6.9
GO:0051092	pos. reg. of NF-kappaB transcription factor activity	4.5E-05	1.9E-03	2.7
GO:0042110	T cell act.	5.1E-08	4.9E-06	2.8
GO:0042098	T cell proliferation	3.3E-04	1.1E-02	4.0
GO:0030217	T cell diff.	4.4E-05	1.9E-03	2.9

Down Regulated Gene-Enriched

GO Term	Description	P-value	FDR q-value	Enrichment
GO:1903047	mitotic cell cycle process	2.9E-38	4.1E-34	3.5
GO:0034080	CENP-A containing nucleosome assembly	1.3E-07	3.9E-05	5.9
GO:0045841	neg. reg. of mitotic metaphase/anaphase trans.	9.8E-05	1.1E-02	4.6
GO:1902100	neg. reg. of metaphase/anaphase trans. of cell cycle	1.2E-04	1.3E-02	4.5
GO:2000816	neg. reg. of mitotic sister chromatid separation	4.6E-06	8.2E-04	5.2
GO:0033048	neg. reg. of mitotic sister chromatid segregation	7.7E-06	1.3E-03	5.0
GO:0033046	neg. reg. of sister chromatid segregation	1.9E-06	3.8E-04	5.2
GO:2001251	neg. reg. of chromosome organization	1.9E-06	3.8E-04	3.3
GO:0051784	neg. reg. of nuclear division	2.4E-05	3.5E-03	3.9
GO:0045839	neg. reg. of mitotic nuclear division	1.5E-05	2.3E-03	4.3
GO:0010948	neg. reg. of cell cycle process	2.2E-09	1.1E-06	2.9
GO:1901988	neg. reg. of cell cycle phase trans.	4.2E-07	1.0E-04	3.0
GO:0006260	DNA replication	1.8E-11	1.4E-08	3.8
GO:1901991	neg. reg. of mitotic cell cycle phase trans.	4.2E-06	7.6E-04	2.8
GO:0045930	neg. reg. of mitotic cell cycle	1.6E-08	6.3E-06	2.9
GO:0045786	neg. reg. of cell cycle	2.9E-09	1.3E-06	2.3
GO:0007094	mitotic spindle assembly checkpoint	6.1E-05	7.7E-03	4.9

B

Class	Description	Number of Genes in Class	% of All Genes in Class
WG	Whole Genome	21431	100.0%
I	Initial Cytokine or Effector Response	24	0.1%
II	Preparation for Cell Division	498	2.3%
III	Cell Cycle % Cell Division	231	1.1%
IV	Naïve and Late Memory	65	0.3%
V	Early Effector, Late Memory	177	0.8%
VI	Short-term Effector and Memory	45	0.2%
VII	Memory Precusor	81	0.4%
VIII	Naïve or Late Effector or Memory	194	0.9%
IX	Short-term Effector or Memory	72	0.3%
X	Late Effector or Memory	75	0.3%

Figure S1. Summary of Enriched GO terms and T-cell Activation Gene Behaviour Categories used for Figure 1. See also Fig. 1.

Figure S2

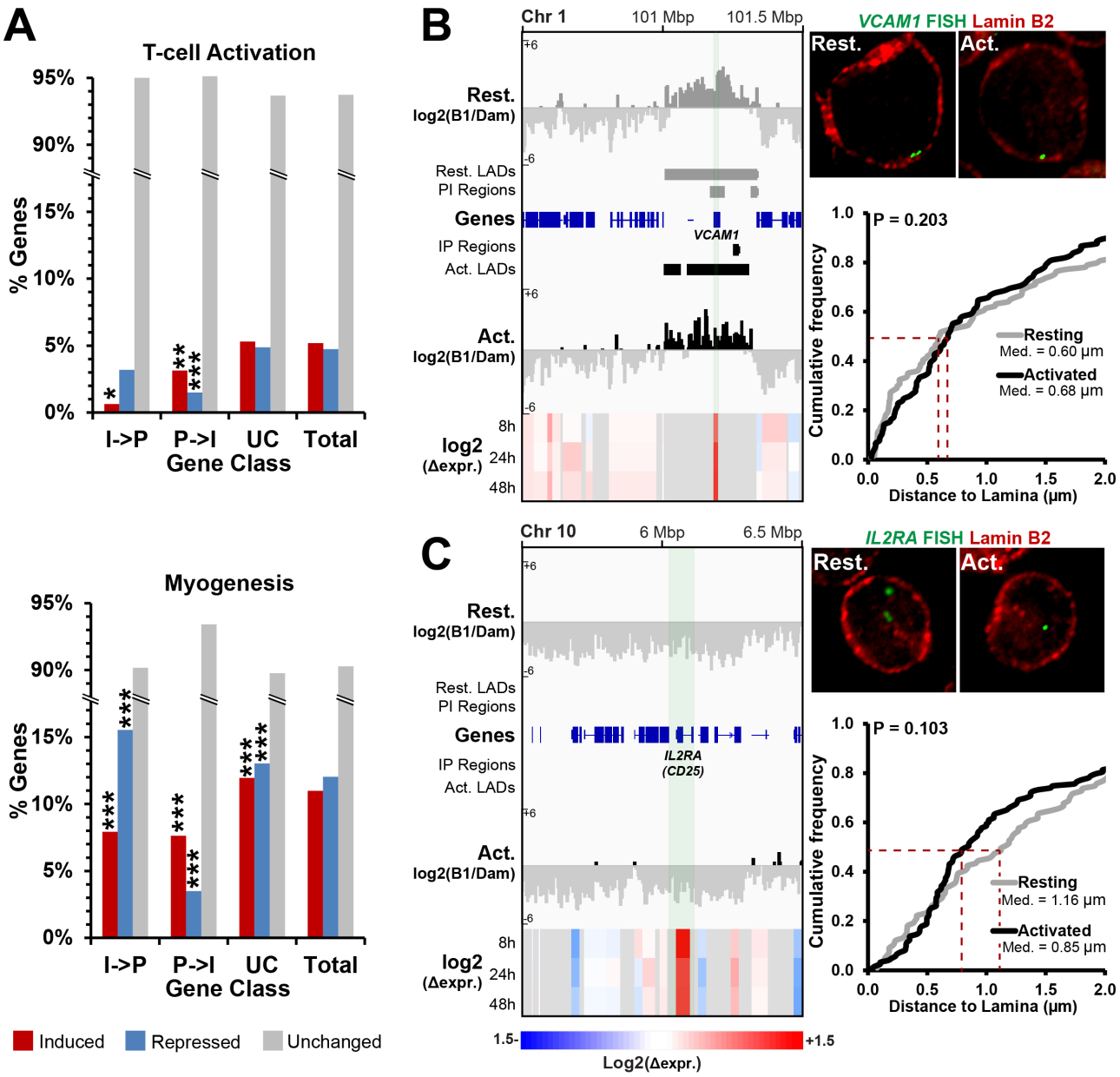

Figure S2. Comparison of T-cell Activation- and Myogenesis-Induced Gene Expression and Repositioning Changes and Additional Gene Peripheral Positioning Quantification. A. Bar graphs displaying gene expression change behaviour of IP, PI, unchanged (UC) and all genes during T-cell activation and myogenesis. For both T-cell activation and myogenesis more PI genes are activated and repressed while more IP genes are repressed than activated. However, fewer repositioning genes display gene expression changes during T-cell activation than in myogenesis. B and C. Genome browser views for the genomic region surrounding *VCAM1* and *CD25*, respectively, and quantification of loci positioning relative to lamin B2. DamID signal intensities, identified LADs, IP and PI regions and microarray gene expression changes for Resting and Activated Jurkat T-cells are shown. B. The *VCAM1* locus which contains both IP and PI regions displays no significant release from the periphery during T-cell activation. C. The consistently non-LAD *CD25* locus is signeifciantly further from the periphery and displays no significantly altered positioning following activation. For quantification statistics, the position of loci in the activated sample were compared to the resting sample by KS tests. *$P < 0.05$, **$P < 0.01$ and *** $P < 0.001$. See also Figure 2 and 3.

Figure S3

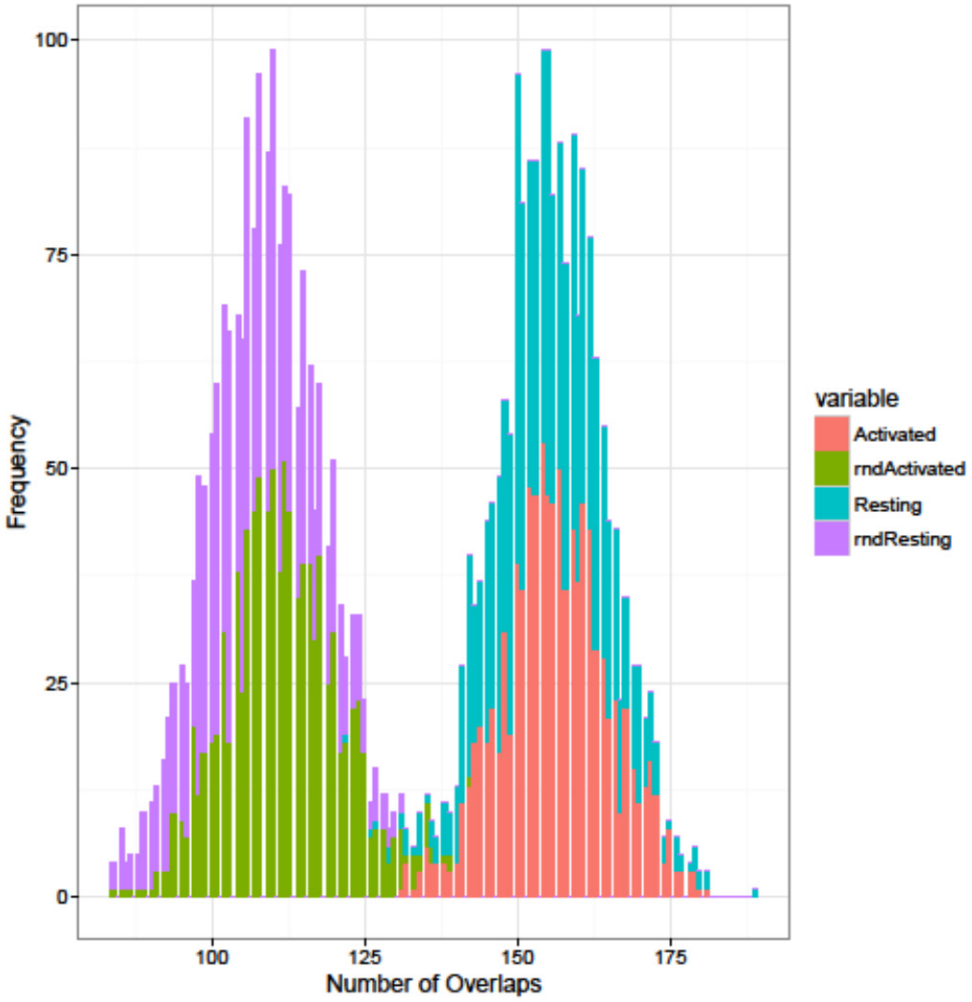

Figure S3. LADs are frequently encompassed within TADs. In order to accurately compare the overlap between LADs and TADS in both resting and activated cells, the number of LADs in each file was down-sampled randomly to 500 features and the number of times a LAD was found completely within a TAD was counted. Then the location of each LAD per chromosome in the down-sampled files was randomized and the number of overlaps to TADs counted. This process was repeated 1,000 times in order view the distribution of overlaps in randomized and non-randomized LAD/TAD overlaps. No differences could be detected between activated and resting cells; however there were non-overlapping distributions for LADS that were found completely within TADS between randomized and observed results. This indicates that these events are significantly enriched over what is expected by random chance.

Figure S4

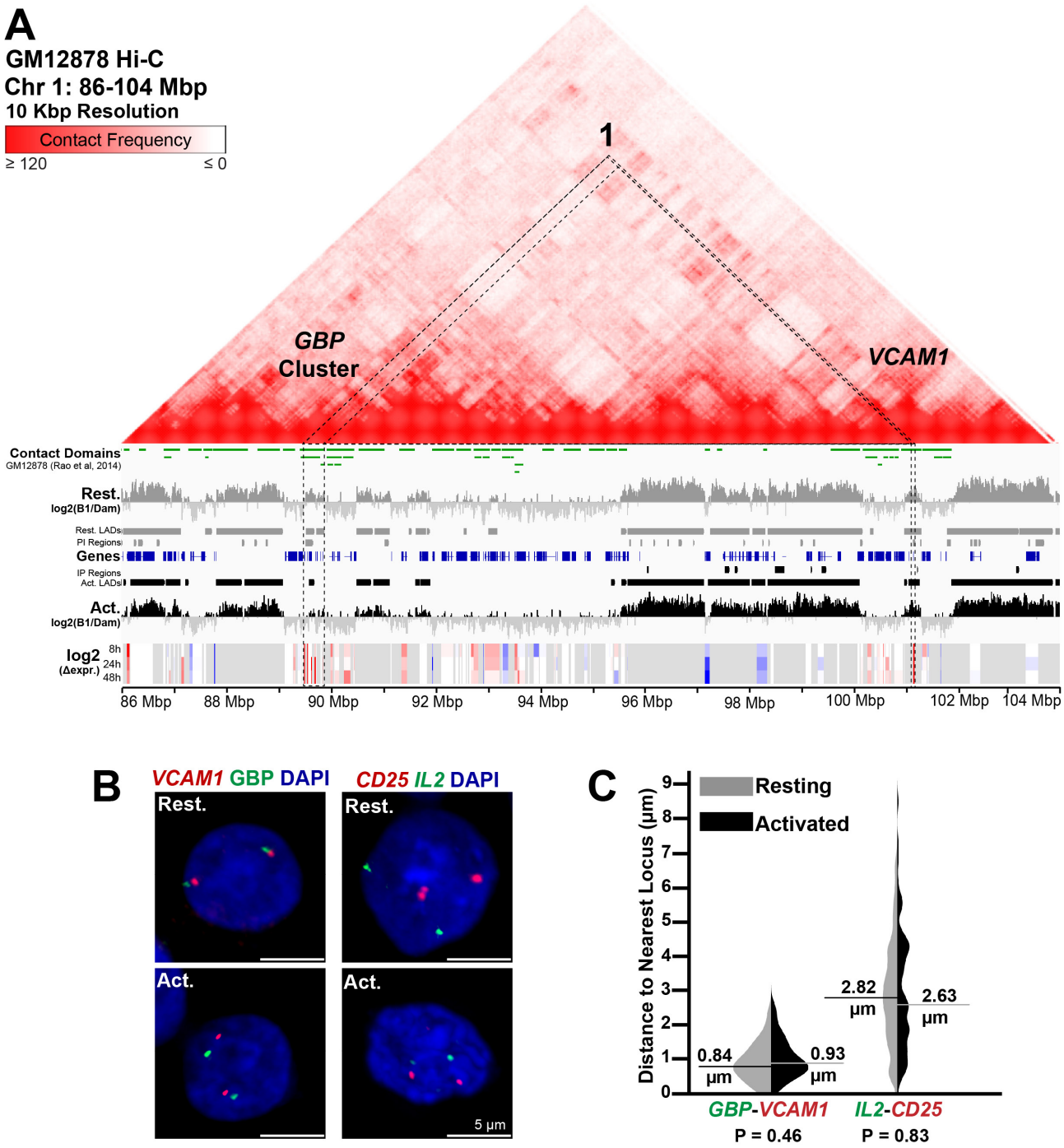

Figure S4. Quantification of the Spatial Separation of Distal Intra-Chromosomal Loci or Inter-Chromosomal Loci which Lack Hi-C Interactions. A. Genome browser view of a 17 Mbp region of chromosome 1 with GM12878 cell Hi-C interactions (ref) and Contact Domains, DamID signal intensities, identified LADs, IP and PI regions and microarray gene expression changes for Resting and Activated Jurkat T-cells displayed. The GBP cluster and *VCAM1* display no observable Hi-C interaction. B and C. Representative images and quantification of inter-loci distances in resting and activated T-cells for the *VCAM1* and the *GBP* gene cluster and the *CD25* and *IL2* loci. The distance between *CD25* and *IL2* and the more spatial proximal *VCAM1* and the *GBP* gene cluster remains unchanged during T-cell activation. For quantification statistics, the positions of loci in the activated sample were compared to the resting sample by KS tests. **P* < 0.05, **P < 0.01 and *** *P* < 0.001.